

Multifractality and Rainfall Extremes: A Review

Daniele Veneziano¹, Andreas Langousis¹ and Pierluigi Furcolo²

¹Department of Civil and Environmental Engineering
Massachusetts Institute of Technology
Cambridge, Massachusetts 02139

²Dipartimento di Ingegneria Civile
Universita' degli Studi di Salerno, Fisciano (SA), Italy

Submitted to

Water Resources Research
Special Issue on *Rain, Rivers and Turbulence*

Revised
March, 2006

Correspondence: Dept. of Civil and Environmental Engineering, MIT, Room 1-348, Cambridge, MA 02139. Phone : (617)253-7199, Fax: (617)253-6044, e-mail: venezian@mit.edu

Abstract

The multifractal representation of rainfall and its use to predict rainfall extremes have advanced significantly in recent years. This paper summarizes this body of work and points at some open questions. The need for a coherent overview comes in part from the use of different terminology, notation and analysis methods in the literature and in part from the fact that results are dispersed and not always readily available. Two important trends have marked the use of multifractals for rainfall and its extremes. One is the recent shift of focus from asymptotic scaling properties (mainly for the intensity-duration-frequency curves and the areal reduction factor) to the exact extreme distribution under non-asymptotic conditions. This shift has made the results more relevant to hydrologic applications. The second trend is a more sparing use of multifractality in modeling, reflecting the limits of scale invariance in space-time rainfall. This trend has produced models that are more consistent with observed rainfall characteristics, again making the results more suitable for application. Finally we show that rainfall extremes can be analyzed using rather rough models, provided the parameters are fitted to an appropriate range of large-deviation statistics.

Keywords: rainfall extremes, intensity-duration-frequency curves, areal reduction factor, scale invariance, multifractal processes

1. Introduction

Hydrologic risk analysis and design are often controlled by extreme precipitation events. This is why the evaluation of rainfall extremes, which is commonly embodied in the intensity-duration-frequency (IDF) and intensity-duration-area-frequency (IDAF) curves, has been a major focus of theoretical and applied hydrology for many decades (*Sherman, 1931; Bernard, 1932; Eagleson, 1970; Chow et al., 1988; Burlando and Rosso, 1996; Sivapalan and Blöschl, 1998; Koutsoyiannis et al., 1998; Willems, 2000; Menabde and Sivapalan, 2000; Asquith and Famiglietti, 2000; Veneziano and Furcolo, 2002a; Castro et al., 2004; Veneziano and Langousis, 2005a*).

A significant body of empirical work (*Schertzer and Lovejoy, 1987; Lovejoy and Schertzer, 1995; Olsson et al., 1993; Gupta and Waymire, 1993; Marsan et al., 1996; Over and Gupta, 1996; Menabde et al., 1997; Harris et al., 1998; Venugopal et al., 1999a; Deidda et al., 1999*, among others) has shown that rainfall in time and space has multifractal scale invariance within finite but practically important ranges, typically from below 1 hour to several days in time and from below 1 km to more than 100 km in space. Other rainfall features that are of particular interest for extremes are that, to a first approximation, the IDF curves display a power-law dependence on averaging duration d and return period T (*Burlando and Rosso, 1996; Willems, 2000*) and the areal reduction factor (ARF) has power-law form over a certain range of averaging area a and duration d (*NERC, 1975; De Michele et al., 2001*) Recent studies (*Hubert et al., 1998; Veneziano and Furcolo, 2002a; Veneziano and Langousis, 2005a*) have shown that these properties are consistent with multifractal scale invariance of the underlying rainfall process. Hence the premises exist to making multifractal modeling a cornerstone of rainfall extreme analysis.

This paper is a tutorial account of rainfall extremes using multifractal models. The exposition is largely shaped by the views and past and ongoing work by the authors. An attempt is made to make the presentation concise but self-contained, with occasional pointers to the literature for detailed derivations and in-depth coverage of certain topics. Proofs of important results are given or at least sketched.

The paper includes three main sections: Section 2 is an introduction to multifractality and the various interpretations of this term that are found in the literature. Emphasis is on the definition of multifractality as a scale invariance property that extends the classic concept of self-similarity. The aim of this section is to provide a general view of multifractal processes while introducing notation and basic results for what follows. Section 3 focuses on the important class of stationary multifractal measures, which are relevant to the modeling of rainfall. Special attention is given to the marginal and extreme properties of these measures. We show how the upper quantiles of the marginal distribution scale with the averaging duration d and the exceedance probability P as either d or P approaches zero, examine the implications of multifractality on the areal reduction factor, and describe numerical procedures to calculate marginal and maximum distributions under non-asymptotic conditions. These results are at the core of the multifractal theory of rainfall extremes.

Section 4 proposes some multifractal models for temporal rainfall and derives their extreme properties. The models are in many ways simplistic, but when properly fitted to data suffice for the estimation of rainfall extremes. Using results from Section 3, we derive the intensity-duration-frequency curves for each model and present an application example. Conclusions and suggestions for future research are given in Section 5.

2. Multifractality – What is it?

An unfortunate state of affairs with multifractality is that there is no general consensus on its definition. The term multifractality has its origin in the fact that different sets extracted from the object of interest, here a random process or a random measure, have different fractal dimensions. Specifically, following *Parisi and Frisch (1985)*, a stationary multifractal measure is singular of order γ on a fractal set whose fractal dimension $D(\gamma)$ depends on γ . Roughly speaking, a singularity of order γ exists at point \underline{t} if the average measure density ε_r in a cube of side length $1/r$ centered at \underline{t} behaves like $r^{-\gamma}$ as the resolution $r \rightarrow \infty$. This “geometric” multifractal property is characterized by the singularity spectrum $D(\gamma)$ or any of several equivalent functions.

For realizations of important classes of random measures one would like to call multifractal (including those most often used to represent rainfall), the local singularity exponent γ at point \underline{t} does not exist. This fact makes it necessary to use a broader “probabilistic” level-exceedance notion of multifractality, as follows. Cover the support of the measure with cubes of side length $1/r$ and let $E[N(r, \gamma)]$ be the expected number of cubes where the average measure density exceeds $r^{-\gamma}$. The measure is multifractal if, for some non-constant $D(\gamma)$, $E[N(r, \gamma)]$ behaves like $r^{D(\gamma)}$ as $r \rightarrow \infty$ (*Schertzer and Lovejoy, 1987, 1996*). Here $D(\gamma)$ is not the fractal dimension of any set; rather, it is an asymptotic fractal-like property of the sequence of $r^{-\gamma}$ -exceedance sets obtained by fixing γ and increasing the resolution r . $D(\gamma)$ is still called the singularity spectrum or dimension function of the measure. Both the geometric and probabilistic level-exceedance definitions of multifractality have been applied mainly to stationary measures.

When using the level-exceedance definition, one often works with the co-dimension function $C(\gamma) = D - D(\gamma)$, where D is the Euclidean embedding dimension ($D = 1$ for measures on a line, $D = 2$ for measures on a plane, etc.). The reason is that the property $E[N(r, \gamma)] \sim r^{D(\gamma)}$ may be restated as $P[\varepsilon_r > r^\gamma] \sim r^{-C(\gamma)}$ where ε_r is the average measure density in a cube of side length $1/r$.

An important implication of the above definitions of multifractality is that, as $r \rightarrow \infty$, the moments of ε_r scale as $E[\varepsilon_r^q] \sim r^{K(q)}$, where $K(q)$ is the Legendre transform of $C(\gamma)$,

$$\begin{aligned} K(q) &= \max_{\gamma} \{q\gamma - C(\gamma)\} \\ C(\gamma) &= \max_q \{q\gamma - K(q)\} \end{aligned} \tag{1}$$

A derivation of Eq. 1 is given in *Schertzer and Lovejoy* (1996), pp. 55-56; see also Section 3 and Appendix A below. If the moment scaling function $K(q)$ is nonlinear, the measure is multifractal; if $K(q)$ is linear but does not pass through the origin, the measure is monofractal; and if $K(q)$ is linear through the origin, the measure is self-similar. Due to the correspondence between level-exceedance and moment-scaling properties in Eq. 1, multifractality is sometimes referred to as the property that the moments of ε_r depend on resolution r as $E[\varepsilon_r^q] \sim r^{K(q)}$ with $K(q)$ a nonlinear function of q .

Some, including the authors, view the above level-crossing and moment-scaling properties as manifestations of a fundamental scale invariance condition called stochastic self-similarity (*sss*), which extends the classical notion of self-similarity (*ss*). Next we recall the definitions of *ss* and *sss* for a (stationary or nonstationary, signed or unsigned) random measure $X(\Omega)$, $\Omega \subset R^D$. The properties are stated in terms of the measure density $\varepsilon(\Omega) = X(\Omega)/|\Omega|$, as $\varepsilon(\Omega)$ is the quantity most often used in multifractal analysis. We consider random measures (also called

generalized random functions; see for example *Yaglom, 1986*) rather than ordinary random processes $X(\underline{t})$ because the latter are special cases of the former and multifractal models of rainfall exist only as random measures. For ordinary processes $X(\underline{t})$, just replace $\varepsilon(\Omega)$ and $\Omega \subset R^D$ with $X(\underline{t})$ and $\underline{t} \in R^D$.

As is well-known (see for example *Samorodnitsky and Taqqu, 1994, Ch. 7*), $X(\Omega)$ is self-similar if constants a_r exist such that, for any $r > 0$,

$$\varepsilon(\Omega) \stackrel{d}{=} a_r \varepsilon(r\Omega) \quad (2)$$

where $\stackrel{d}{=}$ denotes equality of all finite-dimensional distributions. Since $a_{r_1 r_2} = a_{r_1} a_{r_2}$ and $a_1 = 1$, it must be $a_r = r^{-H}$ for some real H and Eq. 2 may be stated more explicitly as

$$\varepsilon(\Omega) \stackrel{d}{=} r^{-H} \varepsilon(r\Omega) \quad (3)$$

The condition of stochastic self-similarity or *sss* differs from Eq. 2 in two respects: 1) the deterministic factors a_r are replaced with random variables A_r , and 2) the range of r over which scale invariance applies is reduced to either $0 < r \leq 1$ (*sss* under dilation or *dsss*) or $r \geq 1$ (*sss* under contraction or *csss*). This leads to the following definition.

A random measure $X(\Omega)$, $\Omega \subset R^D$, is stochastically self-similar if non-negative random variables A_r exist such that

$$\varepsilon(\Omega) \stackrel{d}{=} A_r \varepsilon(r\Omega), \quad \begin{cases} \text{for any } 0 < r \leq 1 & (\text{dsss}) \\ \text{for any } r \geq 1 & (\text{csss}) \end{cases} \quad (4)$$

Gupta and Waymire (1990) and *Veneziano (1999)* have suggested that the scaling property in Eq. 4 be used to define multifractality.

According to the *sss* definition, multifractality is characterized by the marginal distribution of the variables A_r . Important properties of these distributions are listed below. Properties 1 and

2 follow directly from Eq. 4, whereas Properties 3, 4 and 5 follow from the consistency condition

$A_{r_1 r_2} \stackrel{d}{=} A_{r_1} A_{r_2}$, which must hold for any r_1 and r_2 in the allowed range (larger than 1 for *csss* processes, between 0 and 1 for *dsss* processes):

1. For $r = 1$, $A_1 = 1$ with probability 1;
2. For measure densities with constant nonzero mean, $E[A_r] = 1$;
3. $\log(A_r)$ has infinitely divisible distribution, meaning that for any given integer $k > 1$, a random variable B_k exists such that $\log(A_r)$ has the same distribution as the sum of k independent copies of B_k . On infinitely divisible distributions, see for example *Feller* (1968);
4. Let $\varphi_r(t)$ be the characteristic function of A_r . The relationship $\varphi_{r_1}(t) = [\varphi_{r_2}(t)]^{\log(r_1)/\log(r_2)}$, which holds for any $1 < r_2 < r_1$ in the *csss* case and any $0 < r_1 < r_2 < 1$ in the *dsss* case, allows one to find the distribution of A_{r_1} from the distribution of A_{r_2} . Therefore it suffices to know the distribution of A_r for just one value of r ;
5. The non-diverging moments of A_r and $\mathcal{E}(\Omega)$ scale with r as

$$\begin{aligned} E[A_r^q] &= r^{K(q)} \\ E[\mathcal{E}(\Omega/r)^q] &\propto r^{K(q)} \end{aligned} \tag{5}$$

where $K(q)$ is a convex function. Equation 5 shows that the *sss* definition of multifractality reproduces the moment-scaling property of other definitions, but is not limited to stationary measures. As we shall see in Section 3, also the fractal-like property of the level-exceedance sets is reproduced.

Other remarks on *sss* measures:

1. For $r \rightarrow \infty$ (in the case of *csss* measures) or $r \rightarrow 0$ (in the case of *dsss* measures), the variable A_r becomes degenerate, being either 0 or ∞ with probability 1. This implies that, in order for $\mathfrak{a}(\Omega)$ itself to be non-degenerate, the *csss* property must hold below some finite maximum scale Ω_{\max} and the *dsss* property must hold above some non-zero minimum scale Ω_{\min} . As we show in Section 4, the outer scale Ω_{\max} plays an important role in the modeling of rainfall and its extremes.
2. For measures on the line, scaling of the support is expressed by the transformation $rt \rightarrow t$. In higher-dimensional spaces, a direct generalization is $r\mathbf{t} \rightarrow \mathbf{t}$, which corresponds to isotropic expansion/contraction of Ω from the origin. One may consider *ss* and *sss* scale invariance under more general space transformations that for example include rotation or anisotropic scaling of the support (see concept of generalized scale invariance in *Schertzer and Lovejoy, 1991*). For rainfall, anisotropic scaling in space and time is often referred to as “dynamic scaling”. The degree to which rainfall exhibits dynamic or other generalized type of scaling is however unclear and conflicting results have been reported (*Marsan et al., 1996; Venugopal et al., 1999b; Deidda, 2000; Deidda et al., 2004*). As the most extensive analyses to date (*Deidda, 2000; Deidda et al., 2004*) favor isotropy, here we deal exclusively with isotropic scaling.

In spite of many similarities, the definitions of multifractality given above are not completely equivalent. In our view, the *sss* concept is more fundamental and intuitive than the fractal-like property of a sequence of random level-exceedance sets and makes multifractality a natural extension of self-similarity. For these reasons, in all that follows we adopt the *sss* notion of multifractality.

3. Stationary Multifractal Measures and Their Marginal and Extreme Properties

Next we focus on the class of (non-negative) stationary measures, which are especially relevant to rainfall modeling. Such measures can be *csss* but not *dsss* and are *ss* (with $H = 0$) only in the uninteresting case of uniform measures.

We review many classic and recent results on stationary *sss* measures. In Section 3.1 we give a general procedure to construct stationary *sss* measures and discrete multiplicative cascades, which are models with limited stationarity and *sss* properties. Discrete cascades are of interest because they are simpler to analyze and produce results that are often identical or close to those of continuous-scaling measures. Section 3.2 focuses on the marginal properties of discrete cascades, including the moments, marginal distribution and extreme quantiles of $\mathfrak{a}(\Omega)$. Methods to calculate the distribution of the maximum of $\mathfrak{a}(\Omega)$ inside the region of multifractal scaling Ω_{\max} are given in Section 3.3.

3.1 Construction of Stationary Multifractal Measures and Discrete Cascades

(a) *Continuous-scaling Measures*

Suppose that Ω_{\max} is the unit D -dimensional cube $\Omega_0 = \{\underline{t} : 0 \leq t_i \leq 1, i = 1, \dots, D\}$. Stationary *sss* measures in Ω_0 are obtained as products of scaled independent copies of a non-negative stationary process. Specifically, let $r_o > 1$ be a scale-change factor and $W_{r_o}(\underline{t})$, $\underline{t} \in R^D$, be a stationary process such that $W_{r_o}(\underline{t})$ may be considered constant inside Ω_0 and $E[e^{W_{r_o}}] = 1$. For any positive integer n , define an ordinary random process $X_{r_o, n}(\underline{t})$ and the associated measure density $\varepsilon_{r_o, n}(\Omega)$ as

$$\begin{aligned}
X_{r_o,n}(\underline{t}) &= \exp\left\{\sum_{i=1}^n W_{r_o,i}(r_o^i \underline{t})\right\} \\
\varepsilon_{r_o,n}(\Omega) &= \frac{1}{|\Omega|} \int_{\Omega} X_{r_o,n}(\underline{t}) d\underline{t}
\end{aligned} \tag{6}$$

where the random processes $W_{r_o,i}(\underline{t})$ are independent copies of $W_{r_o}(\underline{t})$. As $n \rightarrow \infty$, $X_{r_o,n}(\underline{t})$ becomes singular, but under conditions on the marginal distribution of W_{r_o} given below, $\varepsilon_{r_o,n}(\Omega)$ converges to a non-degenerate measure density $\varepsilon_{r_o}(\Omega)$ with the *sss* property

$$\varepsilon_{r_o}(\Omega) \stackrel{d}{=} e^{W_{r_o}} \varepsilon_{r_o}(r_o \Omega), \quad r_o \Omega \subset \Omega_0 \tag{7}$$

Notice that $\varepsilon_{r_o}(\Omega)$ is *sss* only under contraction by the discrete set of factors $r = r_o^n$, $n = 0, 1, \dots$. To obtain a measure that is *sss* under any $r > 1$, one must constrain $W_{r_o}(\underline{t})$ to be an infinitely divisible process and “densify” the previous construction in scale, as follows. For a random process $W_{r_o}(\underline{t})$, infinite divisibility means that, for any integer $k > 1$, $W_{r_o}(\underline{t})$ may be represented as the sum of k independent copies $W_{r_o^{1/k},i}(\underline{t})$ of some other random process $W_{r_o^{1/k}}(\underline{t})$. Then one replaces Eq. 6 with

$$\begin{aligned}
X_{r_o^{1/k},nk}(\underline{t}) &= \exp\left\{\sum_{i=1}^{nk} W_{r_o^{1/k},i}(r^{i/k} \underline{t})\right\} \\
\varepsilon_{r_o^{1/k},nk}(\Omega) &= \frac{1}{|\Omega|} \int_{\Omega} X_{r_o^{1/k},nk}(\underline{t}) d\underline{t}
\end{aligned} \tag{8}$$

Taking the limit of $\varepsilon_{r_o^{1/k},nk}(\Omega)$ for $n,k \rightarrow \infty$ produces a continuous-scaling *csss* measure density $\varepsilon(\Omega)$ that satisfies Eq. 4 for any $r \geq 1$, with $A_{r_o} = e^{W_{r_o}}$.

In some cases one can construct stationary *sss* measures using more direct methods. A notable example is when $W_{r_o}(\underline{t})$ is a normal process, implying that also $\ln[X_{r_o^{1/m},nk}(\underline{t})]$ is a normal process. One can see from Eq. 8 that, for measures in D -dimensional space, as $n,k \rightarrow \infty$

the spectral density of $\ln[X_{r_o^{1/k}, nk}(\underline{t})]$ approaches a function $S_{\ln X}(\underline{\omega})$ that for frequencies $|\underline{\omega}|$ larger than some lower limit ω_o decays like $|\underline{\omega}|^{-D}$ in any given direction from the origin. This property can be used to characterize and simulate the measure density $\varepsilon(\Omega)$. *Schertzer and Lovejoy* (1991) and *Wilson et al.* (1991) have extended this spectral construction method to the case when $W_{r_o}(\underline{t})$ is a stable non-normal process.

(b) Discrete Cascades

Discrete *sss* cascades (*Mandelbrot*, 1974; *Schertzer and Lovejoy*, 1987; *Gupta and Waymire*, 1993) are obtained through a simpler procedure, in which:

- r_o is a positive integer $m > 1$, called the (linear) multiplicity of the cascade. For cascades, we use m rather than r_o to emphasize that the multiplicity is an integer;
- R^D is partitioned into unit cubic tiles and $W_m(\underline{t})$ has constant *iid* values in different tiles;
- No densification is made ($k = 1$).

Hence the construction of a discrete cascade in Ω_0 proceeds in steps. At step n , each cubic tile at the previous step ($n - 1$) is partitioned into m^D cubic sub-tiles and the measure density in each sub-tile is multiplied by an independent variable with the distribution of $A_m = e^{W_m}$. Figure 1a illustrates the partition of Ω_0 into square tiles for the case $D = 2$ and $m = 2$. Figure 1b shows a realization when W_2 has normal distribution with mean value $-0.1\ln(2)$ and variance $0.2\ln(2)$ and the cascade construction has reached resolution level $n = 9$. Discrete cascades are not quite stationary (marginal and joint distributions are invariant with respect to a discrete set of translations) and have limited *sss* properties (the Ω regions in Eq. 4 must be cascade tiles and r must equal m^n for some non-negative integer n).

A key advantage of working with discrete cascades is that one can unambiguously distinguish between bare and dressed measure densities. These quantities are defined as follows. Let Ω_n be a tile at step n of the cascade construction. The bare density $\varepsilon_{n,b} = \varepsilon_b(\Omega_n)$ is the constant measure density in Ω_n at the end of step n , whereas the dressed density $\varepsilon_n = \varepsilon(\Omega_n)$ is the average measure density in Ω_n for the fully developed cascade. The densities $\varepsilon(\Omega)$ we have considered up to now are dressed. We use a subscript b to denote quantities related to bare densities. Symbols that lack such subscript refer to dressed quantities.

$\varepsilon_{n,b}$ and ε_n have the following distributional properties. The log bare density $\ln(\varepsilon_{n,b})$ is distributed like the sum of n independent copies of W_m (i.e. like W_{m^n}), whereas the dressed density ε_n satisfies

$$\varepsilon_n = Z \varepsilon_{n,b}^d \quad (9)$$

The “dressing factor” Z in Eq. 9 is independent of $\varepsilon_{n,b}$ and has the same distribution as ε_0 , the dressed average density in Ω_0 .

Kahane and Peyriere (1976) have shown that Z is non-degenerate (in the sense that Z is 0 with probability less than 1) if and only if $K_b'(1) < D$, where $K_b'(q)$ is the derivative of the bare moment-scaling function $K_b(q) = \log_m E[e^{qW_m}]$. Due to Eq. 9, this is also the condition for non-degeneracy of the (dressed) cascade.

3.2 Marginal Properties

In this section we obtain important marginal properties of discrete cascades. As before, the cascades are defined inside the unit cube Ω_0 of R^D and have integer linear multiplicity $m \geq 2$. Hence the tiles $\Omega_{n,i}$ at level n of the cascade construction are cubes of side length m^{-n} . Interest is in the distribution of the dressed density ε_n inside a generic tile Ω_n .

(a) Moments of ε_n

Kahane and Peyriere (1976) found that the moment $E[Z^q]$, $q > 1$, exists if and only if $K_b(q) < D(q - 1)$; see also Appendix B. Hence the critical order $q_D^* > 1$ above which the moments $E[\varepsilon_n^q]$ diverge is found from $K_b(q_D^*) = D(q_D^* - 1)$. If no such q_D^* exists, then ε_n has finite moments of all orders $q > 1$. This is important for the extremes because, if q_D^* exists, then the upper tail of ε_n has power-law form $P[\varepsilon_n > \varepsilon] \sim \varepsilon^{-q_D^*}$. An example of moment scaling function $K_b(q)$ (for W_m a normal variable) and associated critical moment order q_D^* is shown in Figure 2a. Next we give a method to calculate the moments $E[\varepsilon_n^q]$ of integer order q between 1 and q_D^* .

It follows from Eq. 9 and $E[\varepsilon_{n,b}^q] = m^{nK_b(q)}$ that

$$E[\varepsilon_n^q] = m^{nK_b(q)} E[Z^q] \quad (10)$$

Hence the problem is to find $E[Z^q]$. These moments are obtained using the fundamental relationship

$$Z = \frac{1}{m^D} \sum_{i=1}^{m^D} A_{m,i} Z_i \quad (11)$$

where all the variables on the right hand side are mutually independent, the variables $A_{m,i}$ are distributed like A_m and the variables Z_i are distributed like Z . Equation 11 follows from $\varepsilon_0 = Z$ and the fact that $\varepsilon_0 = \varepsilon(\mathcal{Q}_0)$ is the average of the m^D iid dressed densities $\varepsilon_{1,i} = \varepsilon(\mathcal{Q}_{1,i}) = A_m Z$.

To find $E[Z^q]$ from Eq. 11, one uses the multinomial expansion of $(\sum_{i=1}^{m^D} A_{m,i} Z_i)^q$ to express $E[(\sum_{i=1}^{m^D} A_{m,i} Z_i)^q]$ as a linear function of moments of Z of order up to q . Then one solves

$E[Z^q] = m^{-qD} E[(\sum_{i=1}^{m^D} A_{m,i} Z_i)^q]$ for $E[Z^q]$ in terms of the lower integer moments of Z and the known moments of A_m . Finally, one finds $E[Z^q]$ recursively for $q = 1, 2, \dots$, starting from $E[Z] = 1$. Details are in *Veneziano and Furcolo (2003)*.

Since $E[Z^q]$ diverges for $q \geq q_D^*$, one can use Eq. 10 to write the dressed moments as $E[\varepsilon_n^q] \sim m^{nK(q)}$, where the dressed moment scaling function $K(q)$ is given by

$$K(q) = \begin{cases} K_b(q), & q < q_D^* \\ \infty, & q \geq q_D^* \end{cases} \quad (12)$$

Note that while $K_b(q)$ does not depend on the space dimension D , $K(q)$ does (through q_D^*); see Figure 2a.

(b) Upper Tail of ε_n for Large n

To characterize the upper tail of ε_n for n large, we consider probabilities of the type $P[\varepsilon_n > m^{n\gamma}]$ for given γ and $n \rightarrow \infty$. We are specifically interested in these probabilities because, as we shall see in Section 3.3, they are linked to the return-period values of ε_n .

Recall from Section 2 that the property $P[\varepsilon_n > m^{n\gamma}] \sim m^{-nC(\gamma)}$ is sometimes taken as the definition of multifractality. This relationship has the form of a rough limit. A more refined characterization of the tail behavior of ε_n is

$$\lim_{n \rightarrow \infty} \frac{P[\varepsilon_n > m^{n\gamma}]}{m^{-nC(\gamma)}} = g(m^n, \gamma) \quad (13)$$

where $g(r, \gamma)$ is a function that varies slowly with r . As we show next, one can derive the function $g(r, \gamma)$ and the Legendre transform relationship between $C(\gamma)$ and $K(q)$ starting from the sss condition in Eq. 4.

Consider first the bare densities $\varepsilon_{n,b}$. One may use Cramer's (refined) Theorem for large deviations of sums of *iid* random variables (Cramer, 1938; see also Dembo and Zeitouni, 1993, or Varadhan, 1984) to obtain

$$\lim_{n \rightarrow \infty} \frac{P[\varepsilon_{n,b} > m^{n\gamma}]}{m^{-nC_b(\gamma)}} = g_b(m^n, \gamma) \quad (14)$$

where $C_b(\gamma)$ is the Legendre transform of $K_b(q) = \log_m E[A_m^q]$ and $g_b(r, \gamma) = \left[2\pi \frac{[C_b'(\gamma)]^2}{C_b''(\gamma)} \ln(r) \right]^{-1/2}$; see Veneziano (2002). The link to large deviations for sums of *iid* variables is through the fact that the log bare density $\ln(\varepsilon_{n,b})$ is the sum of n *iid* variables distributed like W_m . A more direct proof of Eq. 14 is given in Appendix A.

Veneziano (2002) has extended the previous result to the dressed densities ε_n . In this case Eq. 13 holds with $C(\gamma)$ the Legendre transform of $K(q)$ in Eq. 12,

$$C(\gamma) = \begin{cases} C_b(\gamma), & \gamma \leq \gamma_D^* \\ q_D^* \gamma - D(q_D^* - 1), & \gamma > \gamma_D^* \end{cases} \quad (15)$$

and $g(r, \gamma)$ given by

$$g(r, \gamma) = \begin{cases} E[Z^{C_b(\gamma)}] \left(2\pi \frac{[C_b'(\gamma)]^2}{C_b''(\gamma)} \ln(r) \right)^{-1/2}, & \gamma < \gamma_D^* \\ \lim_{z \rightarrow \infty} \frac{P[Z > z]}{z^{-q_D^*}}, & \gamma > \gamma_D^* \end{cases} \quad (16)$$

The constant $\gamma_D^* = K_b'(q_D^*)$ in Eqs. 15 and 16 is the value of γ associated with q_D^* ; see Figure 2.

Equations 13, 15 and 16 may be written in more compact form as

$$P[\varepsilon_n \geq m^{n\gamma}] \approx \begin{cases} P[\varepsilon_{n,b} \geq m^{n\gamma}] E[Z^{C(\gamma)}], & \gamma < \gamma_D^* \\ P[Z \geq m^{n\gamma}] E[\varepsilon_{n,b}^{C(\gamma)}] = P[Z \geq m^{n\gamma}] m^{nD(q_D^* - 1)}, & \gamma > \gamma_D^* \end{cases} \quad (17)$$

where \approx denotes equality up to a factor that approaches 1 as $n \rightarrow \infty$ and $C'(\gamma)$ is the moment order q associated with γ in the dressed cascade. Equation 17 emphasizes the symmetrical roles played by the factors $\varepsilon_{n,b}$ and Z in determining the exceedance probability $P[\varepsilon_n \geq m^{n\gamma}]$ of $\varepsilon_n = \varepsilon_{n,b}Z$: when $\gamma < \gamma_D^*$, $\varepsilon_{n,b}$ dominates and Z contributes a factor $E[Z^{C'(\gamma)}]$ to the exceedance probability, whereas for $\gamma > \gamma_D^*$, Z dominates and $\varepsilon_{n,b}$ contributes a factor $E[\varepsilon_{n,b}^{C'(\gamma)}] = m^{nK(q_D^*)} = m^{nD(q_D^*-1)}$. Equation 17 will be used in Section 3.3 to study the asymptotic behavior of return-period values of ε_n .

(c) Marginal Distribution of ε_n for any n

Equation 17 characterizes the upper tail behavior of ε_n as $n \rightarrow \infty$, but for many applications one is interested in the entire distribution of ε_n for n finite. Here we give a numerical procedure to find this distribution.

Notice that $\varepsilon_n = \varepsilon_{n,b}Z$ and the distribution of $\varepsilon_{n,b}$ is known, being the same as the distribution of the scaling factor A_{m^n} . The distribution of the dressing factor Z can be obtained from Eq. 11 using the following procedure.

Several distributions F_Z satisfy Eq. 11, for example one with probability mass 1 at $Z = 0$. To find the distribution of the dressing factor, one can use the fact that Z has the distribution of $\varepsilon(\Omega_0)$ and calculate the latter as the cascade construction progresses. This corresponds to iteratively solving Eq. 11 starting from $F_Z^{(0)}(z) = H(z-1)$, the Heaviside unit step function at $z = 1$: first one calculates the distribution $F_Z^{(1)}$ of the right hand side of Eq. 11 assuming that the variables Z_i have distribution $F_Z^{(0)}$ and then one calculates $F_Z^{(2)}$ assuming that the variables Z_i

have distribution $F_Z^{(1)}$, and so on until convergence; see *Veneziano and Furcolo (2003)* for details.

As an example, Figure 3 shows plots of consecutive approximations to the probability density function of Z for a binary cascade ($m = 2$) on the line ($D = 1$), when the scaling factor A_2 has lognormal distribution with mean value 1 and second moment $E[A_2^2] = 2^{0.2}$. In this case the critical order of moment divergence is $q_D^* = 10$. Calculation of F_Z was stopped at iteration 26, when a convergence criterion was met. The integer moments of $Z^{(26)}$ were then calculated numerically and compared with the exact moments based on Eq. 11. The inset in Figure 3 shows the moment ratio $E[Z^q]/E[(Z^{(26)})^q]$ for $q = 1, 2, \dots, 9$. The fact that this ratio is very close to 1 over the whole range of finite moments indicates that good convergence has been reached.

Veneziano and Furcolo (2003) also studied the distribution of ε_n in the small-scale limit $n \rightarrow \infty$. The main result is that, while other possible limiting distributions exist, the lognormal distribution has the largest domain of attraction, for ε_n when $P[A_m = 0] = 0$ and for $(\varepsilon_n | \varepsilon_n > 0)$ when $0 < P[A_m = 0] < 1$. Therefore, at small scales, “almost all” stationary *sss* measures have lognormal or conditional lognormal distribution.

3.3 Extremes

Results of two types are relevant to the problem of cascade extremes: 1. the upper tail of ε_n (which was studied in Section 3.2) and 2. the distribution of $\varepsilon_{n,\max}$, the maximum of the dressed densities $\varepsilon_{n,i}$ over the tiles $\Omega_{n,i}$. While the distribution of $\varepsilon_{n,\max}$ is the result of greater interest, the marginal upper tail provides asymptotic scaling relations for the “return-period value” $\varepsilon_{n,T}$, defined here as the value that is exceeded by ε_n with probability $1/(m^{nD}T)$. Since a cascade in the unit D -dimensional cube Ω_0 contains m^{nD} tiles $\Omega_{n,i}$, $\varepsilon_{n,T}$ is expected to be exceeded once in

T cascade realizations and T may be viewed as the return period of the event $[\varepsilon_n > \varepsilon_{n,T}]$ in units of cascade realizations.

Asymptotic results on $\varepsilon_{n,T}$ are given in Part (a). These results are directly applicable to the IDF curves of temporal rainfall. However, to extend the results to area rainfall averages and for example examine the behavior of the areal reduction factor (ARF), additional theory is needed. This is given in Part (b). Parts (a) and (b) study extremes using marginal distributions and therefore neglect dependence among the measures in different cascade tiles. Part (c) derives the distribution of $\varepsilon_{n,\max}$ accounting for dependence.

(a) Asymptotic Scaling of Return-period Values

Appendix C shows that the return period values $\varepsilon_{n,T}$ scale asymptotically as

$$\varepsilon_{n,T} \sim \begin{cases} m^{n\gamma_D} T^{1/q_D}, & \text{for } n \rightarrow \infty, T \text{ finite} & (a) \\ m^{nD} T^{1/q_D^*}, & \text{for } n \text{ finite}, T \rightarrow \infty & (b) \end{cases} \quad (18)$$

where γ_D is the slope of the tangent to $K(q)$ with Y-intercept equal to $-D$ and q_D is the value of q at the point of tangency; see Figure 2. The result for $(n \text{ finite}, T \rightarrow \infty)$ was first derived by *Hubert et al.* (1998) and the result for $(n \rightarrow \infty, T \text{ finite})$ was obtained by *Veneziano and Furcolo* (2002a). The latter reference also shows that these asymptotic scaling properties do not depend on the precise definition of the return period T and for example still hold when T is defined using the maximum of ε_n inside the unit cube.

To illustrate numerically, Figure 4 shows plots of $\varepsilon_{n,T}$ for the cascade on the line that was used in Figure 3. In this case $D = 1$ and $m = 2$. Other relevant parameters are

$$\begin{aligned} K_b(q) &= 0.1(q^2 - q) & \gamma_1 &= 0.1(2\sqrt{10} - 1) = 0.532 \\ q_1^* &= 10 & q_1 &= \sqrt{q_1^*} = \sqrt{10} = 3.16 \end{aligned} \quad (19)$$

The quantity on the horizontal axis in Figure 4 is the averaging duration $d = 2^{-n}$ and different curves are for different return periods T . The values of $\varepsilon_{n,T}$ are obtained as the $[1 - (2^n T)^{-1}]$ -quantiles of ε_n , calculated numerically using the procedure of Section 3.2 and $Z^{(26)}$ in Figure 3 in place of Z . For small d (large n), the plots confirm the asymptotic scaling result in Eq. 18a. The limiting result in Eq. 18b starts to appear at the coarsest resolution $d = 1$ ($n = 0$) for the longest return period $T = 10^6$. For smaller d , that limiting result holds for such long return periods that it is irrelevant in practice.

(b) Return Period Values in Sub-spaces and the ARF Factor

The results in Eq. 18 apply when one counts the exceedance events $[\mathcal{A}(\Omega_{n,i}) > \varepsilon_{n,T}]$ in all the m^{nD} tiles $\Omega_{n,i}$ that make up Ω_0 , the unit cube in R^D . This is fine for rainfall at a point, for which $D = 1$ and R^D is the time axis. However, for rainfall in two spatial dimensions plus time ($D = 3$), the averaging space-time region is fixed in space and slides in time. In addition, the averaging region is not necessarily a cascade tile. These features require an extension of Eq. 18, as we show next.

To exemplify, suppose that averaging is in a square geographical region of side length $l = m^{-n_s}$ and over a time interval of duration $d = m^{-n_t}$. The dressed density in such space-time region is denoted by ε_{n_s, n_t} , with T -cascade return period value $\varepsilon_{n_s, n_t, T}$. Below we derive asymptotic scaling relations for $\varepsilon_{n_s, n_t, T}$ and for the areal reduction factor (ARF),

$$\eta_{n_s, n_t, T} = \frac{\varepsilon_{n_s, n_t, T}}{\varepsilon_{\infty, n_t, T}},$$

which is the ratio between $\varepsilon_{n_s, n_t, T}$ and the corresponding return period value

at a geographical point, $\varepsilon_{\infty, n_t, T}$. One is interested in this ratio because at many locations the IDF value $\varepsilon_{\infty, n_t, T}$ can be estimated from rain gauge data, whereas lack of space-time rainfall data

makes direct estimation of $\varepsilon_{n_s, n_t, T}$ impossible. If the ARF is insensitive to climate, season etc., then it can be robustly estimated from just one or very few space-time data sets and $\varepsilon_{n_s, n_t, T}$ can be found as the product $\eta_{n_s, n_t, T} \varepsilon_{\infty, n_t, T}$.

By considering rainfall to be multifractal in the unit cube Ω_0 , one implicitly assumes that the units of length and time are such that the outer limit of multifractal behavior is 1 in all spatial and temporal directions. Now let Δn be an integer such that $m^{\Delta n}$ is about 5. *Veneziano and Furcolo* (2002b) have shown that, when n_s and n_t differ by at least Δn ,

$$\varepsilon_{n_s, n_t} \approx \begin{cases} \varepsilon_{\infty, n_t}, & \text{for } n_s > n_t + \Delta n \\ \varepsilon_{n_s, n_s + \Delta n}, & \text{for } n_t > n_s + \Delta n \end{cases} \quad \begin{matrix} (a) \\ (b) \end{matrix} \quad (20)$$

One concludes from Eq. 20a that, when time averaging dominates (when $n_s > n_t + \Delta n$), $\varepsilon_{n_s, n_t, T} \approx \varepsilon_{\infty, n_t, T}$ and $\eta \approx 1$.

A more interesting case is when spatial averaging dominates ($n_t > n_s + \Delta n$). A slight extension of the analysis in Appendix C shows that Eq. C4 in that appendix holds also for rectangular averaging regions with different side lengths, provided their shape is kept constant. This is the case with $\varepsilon_{n_s, n_s + \Delta n}$ in Eq. 20b. Then, using Eq. C4 with $D = 3$ and $D' = 1$, one obtains that the return-period values $\varepsilon_{n_s, n_s + \Delta n, T}$ scale as

$$\varepsilon_{n_s, n_s + \Delta n, T} \sim \begin{cases} m^{n_s \gamma_1} T^{1/q_1}, & \text{for } n_s \rightarrow \infty, T \text{ finite}, n_t > n_s + \Delta n \\ m^{n_s (3-2/q_3^*)} T^{1/q_3^*}, & \text{for } n_s \text{ finite}, T \rightarrow \infty, n_t > n_s + \Delta n \end{cases} \quad (21)$$

where γ_1 and q_1 are γ_D and q_D in Figure 2 for $D = 1$. Equation 21 characterizes the asymptotic scaling of the intensity-duration-area-frequency curves when averaging is mainly in space. By comparison, the IDF values for rainfall at a point are (set $n = n_t$ and $D = 1$ in Eq. 18):

$$\varepsilon_{\infty, n_t, T} \sim \begin{cases} m^{n_t \gamma_1} T^{1/q_1}, & \text{for } n_t \rightarrow \infty, T \text{ finite} & (a) \\ m^{n_t} T^{1/q_1^*}, & \text{for } n_t \text{ finite}, T \rightarrow \infty & (b) \end{cases} \quad (22)$$

Hence the areal reduction factor η , which is the ratio between the return period values in Eqs. 21 and 22, behaves as

$$\eta_{n_s, n_t, T} \sim \begin{cases} m^{(n_s - n_t) \gamma_1}, & \text{for } n_s \rightarrow \infty, T \text{ finite}, n_t > n_s + \Delta n & (a) \\ m^{(n_s - n_t) + 2n_s(1 - 1/q_3^*)} T^{(1/q_3^* - 1/q_1^*)}, & \text{for } n_s \text{ finite}, T \rightarrow \infty, n_t > n_s + \Delta n & (b) \end{cases} \quad (23)$$

Like the asymptotic behavior in Eq. 18b, the asymptotic behavior in Eq. 23b is of little practical interest because it requires extremely long return periods T , especially at spatial resolutions $n_s > 0$. By contrast, the limiting behavior in Eq. 23a is observed over ranges of n_s and n_t of engineering significance. Notice that in this case the ARF scales with $m^{(n_s - n_t)}$, which is the ratio between the duration of time averaging and the side length of the geographical averaging region. The constant γ_1 in the exponent is the value of γ for which $C(\gamma) = 1$; see Figure 2. The same constant appears in the scaling of the IDF curves; see Eq. 22a.

Another interesting observation is that, while strictly nonzero, the dependence of the ARF on the return period T may be neglected. In fact η is independent of T in the first limiting case and in the second limiting case (for which dependence of η on T is maximum and which is rarely approached in practice), the exponent of T is very small. For example, for $K_b(q)$ in Eq. 19, one finds $q_1^* = 10$ and $q_3^* = 30$ and the exponent is -0.067 . This theoretical result sheds light on the debate about the effect of T on the ARF: *NERC* (1975) reports a weak effect, whereas *Bell* (1976), *Asquith and Famiglietti* (2000), and *De Michele et al.* (2001) found that η decreases as T increases. ARF charts for routine hydrologic design (e.g. *Leclerc and Schaake*, 1972; *NERC*,

1975; Koutsoyiannis and Xanthopoulos, 1999) typically give η as a function of only the spatial averaging area a and the temporal averaging duration d . The present results support this practice.

One can validate Eq. 23 through either numerical calculation of the marginal distribution of ε_{n_s, n_t} for different n_s and n_t (this can be done through a simple extension of the method in Section 3.2 for cubic regions) or through numerical simulation of 3-dimensional cascades. An example using the latter approach, with $K_b(q)$ in Eq. 19 and $m = 2$, is shown in Figure 5. Figure 5a shows contour lines of the ARF from the simulated rainfall intensities as a function of $l = m^{-n_s}$ and $d = m^{-n_t}$. Consistently with Eq. 23a, the contour lines indicate that ARF is a function only of the ratio $d/l = m^{(n_s - n_t)}$. The dependence on d/l is shown more explicitly in Figure 5b. Since here $m = 2$, the value on the horizontal axis is the difference $(n_t - n_s)$ and Δn is about 2. Notice that for $(n_t - n_s) < -2$ the ARF is essentially 1 and for $(n_t - n_s) > 2$ the ARF scales as $(d/l)^{\eta}$. This validates our conclusion immediately following Eq. 20 as well as the asymptotic result in Eq. 23a.

The ARF depends somewhat on the shape of the averaging region on the geographical plane. Here we have considered the case of square regions. Other cases (very elongated regions, effect of convection of the rain field) are discussed in Veneziano and Langousis (2005a). The same reference shows that Eq. 23 is in good agreement with the empirical behavior of the ARF in NERC (1975). This is so for averaging durations from 30 min to approximately 8 hours and for averaging areas larger than 100 km². For durations longer than 8 hours and the averaging areas considered in N.E.R.C. (1975), time averaging dominates and hence the ARF is very close to 1 as indicated by Eq. 20, whereas for areas smaller than 100km² biases associated with the small raingauge network density become significant, causing the observed rainfall scaling in N.E.R.C. (1975) to deviate from Eq. 23.

(c) Distribution of $\varepsilon_{n,\max}$

While interesting, the previous results are asymptotic and are based on the marginal distribution of ε_n . Therefore they ignore dependence among the dressed densities $\varepsilon_{n,i}$ in different tiles $\Omega_{n,i}$ (on the dependence structure of stationary multifractal measures, see *Cates and Deutsch*, 1987, and *O'Neil and Meneveau*, 1993). A more appropriate approach to the extremes is to calculate the distribution of the maximum $\varepsilon_{n,\max} = \max_i \{\varepsilon_{n,i}\}$ or more in general the distribution of $\varepsilon_{n_s, n_t, \max} = \max_i \{\varepsilon_{n_s, n_t, i}\}$, where n_s and n_t are not necessarily equal. Next we give a numerical method for $\varepsilon_{n,\max}$, the maximum density among all cubic cascade tiles at level n . Calculation of the distribution of $\varepsilon_{n_s, n_t, \max}$ is more difficult and is not considered here.

As was shown in *Veneziano and Langousis* (2005b), the cumulative distribution function $F_{\varepsilon_{n,\max}}$ can be found recursively for $n = 0, 1, \dots$ by noting that $\varepsilon_{0,\max} = \varepsilon_0 = Z$ and, for any $n > 0$, $\varepsilon_{n,\max}$ is the maximum of m^D iid variables distributed like $A_m \varepsilon_{n-1,\max}$. Therefore, working with logs,

$$F_{\log(\varepsilon_{n,\max})} = \begin{cases} F_{\log(Z)}, & n = 0 \\ [F_{\log(\varepsilon_{n-1,\max})} * f_{\log(A_m)}]^{m^D}, & n = 1, 2, \dots \end{cases} \quad (24)$$

where f_X is the probability density function of X and $F * f$ is the convolution $F * f(s) = \int_{-\infty}^{\infty} F(x) f(s-x) dx$. The distribution of Z , which is needed for $\varepsilon_{0,\max}$, can be obtained through the procedure in Section 3.2.

While generally feasible, numerical calculation of the distribution of $\varepsilon_{n,\max}$ is tedious, since it involves repeated convolutions, first to find the distribution of Z and then to implement Eq. 24. One could use approximations that avoid such convolutions. For example, one might replace Z

with a random variable of the A_r type, say with A_{r_Z} where r_Z is chosen to match some moment of Z (the moments of A_{r_Z} are $E[A_{r_Z}^q] = r_Z^{K(q)}$ and the moments of Z can be found as explained in Section 3.1). One might also neglect dependence among the dressed densities $\varepsilon_{n,i}$ in different tiles and replace Eq. 24 with

$$F_{\log(\varepsilon_{n,\max})} \approx [F_{\log(Z)} * f_{\log(A_{m^n})}]^{m^{nD}}, \quad n = 0, 1, \dots \quad (25)$$

Veneziano and Langousis (2005b) evaluated these approximations and found that replacement of Z by A_{r_Z} generally produces accurate results, except in the extreme upper tail where the power-law behavior of the exact distribution of $\varepsilon_{n,\max}$ is lost. By contrast, ignoring dependence among the cascade tiles produces larger errors in the body of the distribution of $\varepsilon_{n,\max}$, but has little effect on the extreme quantiles. The reason why Eq. 25 is accurate in the extreme upper tail of $\varepsilon_{n,\max}$ is that, as $\varepsilon \rightarrow \infty$, the exceedance events $[\varepsilon_{n,i} > \varepsilon]$ become independent (Poisson).

To illustrate, we consider again the problem of estimating the return-period values $\varepsilon_{n,T}$, defined now as the values exceeded by $\varepsilon_{n,\max}$ with probability $1/T$. All cascade parameters are the same as for Figures 3 and 4, and $D = 1$. Figure 6a shows the exact IDF curves, whereas Figure 6b shows approximate results when Z is replaced with A_{r_Z} using a second-moment matching criterion (in this case $r_Z = 2.237$). Figure 6c uses the same approximation of Z and further neglects dependence among the cascade tiles.

First notice that the curves are close to those derived from the marginal distribution (Figure 4), where T was taken to be the reciprocal of the exceedance rate. This is especially true for large T , since for high thresholds the exceedance events become Poisson. For all combinations of $d=m^{-n}$ and T except d close to the outer scale of multifractal behavior D_{\max} (here $D_{\max} = 1$) and T

very large, the return-period value $\varepsilon_{n,T}$ of $\varepsilon_n = \varepsilon_{n,b}Z$ is determined mainly by the distribution of the bare density $\varepsilon_{n,b}$ and any reasonable approximation of Z produces accurate results (compare Figures 6a and 6b). In the region where the tail of Z is important (d close to 1 and T very large), approximating Z with A_{r_z} produces somewhat low return-period values. If in addition one ignores dependence among the cascade tiles (Figure 6c), the IDF values for small durations d become slightly larger than the exact ones. This is true especially for small T . For large T , the assumption of independence is accurate and the approximate results are very close to the exact ones. Also notice that, for $d = 1$, the IDF values in Figures 6b and 6c coincide.

The general conclusion is that all approximations considered, whether based on the marginal distribution (Figure 4), a moment approximation of Z (Figure 6b) or a moment approximation of Z and the independence assumption among the cascade tiles (Figure 6c), are generally accurate. The main exception is that, when making the independence assumption, the return period values for large d and small T are overestimated by about 50%.

4. Multifractal Models for Rainfall Extremes

In further discussing the problem of precipitation extremes, we focus in this section on temporal rainfall. There is general consensus that rainfall in time displays *sss* scaling, at least under certain conditions and within a finite range of scales (for example during rainstorms and for scales between about 20 minutes and a few days). There is little evidence that scaling extends much beyond these limits. This is for example clear from the spectral analysis of rainfall records (*Fraedrich and Larnder, 1993; Olsson et al., 1993; Olsson, 1995*) and from the distribution of dry periods (*Schmitt et al., 1998; Veneziano and Iacobellis, 2002*).

The accurate representation of rainfall is therefore a complex endeavour, but if interest is in the extremes one may get good results also from rough models. The reason is that the extremes

are insensitive to the low rainfall intensities and the dry inter-storm periods. What is important is to recognize the range of scales over which multifractal scale invariance applies and fit the models using relevant extreme statistics; see Section 4.2 below.

4.1 Three Simple Models

Following *Veneziano and Langousis* (manuscript in preparation), we consider three possible representations of temporal rainfall for extreme analysis, which we call Models 1, 2, and 3.

Model 1 has a rather conventional structure. It assumes that storms of random duration D_{\max} and random mean intensity I_b occur at a certain rate and further that not more than one storm contributes significantly to the yearly maximum intensity in d . The reason why we use the symbol D_{\max} for storm duration is that this is also taken to be the outer limit of multifractal behavior in time. Inside each storm, rainfall intensity is assumed to be a stationary *sss* measure. Hence, the parameters of the model are the joint distribution of (D_{\max}, I_b) , the mean number of yearly storm arrivals λ , and the multifractal parameters of the storm interiors, say the distribution of A_r for a given contraction factor $r > 1$ or equivalently the moment scaling function $K(q)$. All parameters may vary seasonally, but for yearly analysis we consider a single stationary model.

Model 2 is simpler in that it partitions the time axis into intervals of fixed duration D_{\max} . Inside each interval, rainfall is modelled in the same way as during a storm in Model 1. Specifically, inside different intervals $D_{\max,i}$ rainfall is stationary *sss* with mean intensities $I_{b,i}$ drawn at random from the same distribution F_{I_b} . Inside all the intervals, the moment scaling function $K(q)$ is the same. Contrary to the storms of Model 1, the intervals of Model 2 cover the entire time axis and therefore include the dry inter-storm periods. Consequently, the functions F_{I_b} and $K(q)$ one estimates from a given data set for Models 1 and 2 are different.

Model 3 is even simpler, since it adjusts the duration D_{\max} and the moment scaling function $K(q)$ of Model 2 such that the mean intensity I_b inside all intervals may be considered a deterministic constant.

It is convenient to cast all three models in the classic exterior/interior format, in which one distinguishes between rainfall characteristics at large (e.g. synoptic) scale from those at smaller scales (e.g. inside storms). For Model 1, the exterior process is a sequence of rectangular pulses with *iid* durations and intensities, while for Model 2 the exterior process is a partition of the time axis into intervals of constant duration D_{\max} with *iid* average intensities $I_{b,i}$. The exterior process for Model 3 is the same as that for Model 2, but with constant deterministic intensity I_b in all the intervals. Figure 7 gives a schematic representation of these different exterior processes. For all three models, the interior process is a stationary multifractal measure, with moment-scaling function $K(q)$ that depends on the model.

4.2 Model Fitting

In fitting the above models to data, one must pay special attention to the events that are influential on the yearly maximum. Hence in Model 1 one must accurately reproduce the upper tail of the conditional distributions of $(I_b | D_{\max})$, in Model 2 one must fit the upper tail of I_b , and in all models one must estimate $K(q)$ with attention to the higher moments. An additional problem when using Model 1 is the identification of storms from continuous rainfall records. These problems are discussed in detail in *Veneziano and Langousis* (manuscript in preparation). Only the main conceptual steps and results are given below. Application is to a 24-yr continuous rainfall record from Florence, Italy (*Becchi and Castelli*, 1989). In all the analyses, we have used the reduced 23-yr record with the year 1966 removed. In November of that year, an exceptional rainfall event occurred whose return period is estimated to be several hundred years.

For the interior process of Model 1, we have examined the moment-scaling properties of rainfall intensity within storms. For estimating $K(q)$, one should not find the moments of $\varepsilon(d)$, the mean rainfall intensity in an interval of duration d , after pooling together all storms of duration $D_{\max} \geq d$, because such method virtually excludes short-duration storms and, more importantly, the intensity distribution varies with storm duration D_{\max} , biasing the moment-scaling results. The appropriate way to infer the scaling properties of rainfall inside storms of different duration is to use the moments of ε_r , where $r = D_{\max}/d$ is the resolution relative to the outer scale of multifractality of each individual storm.

We have found that storm interiors have negligible lacunarity and are well represented by stationary lognormal sss measures with moment scaling function $K(q) = c(q^2 - q)$ where $c = 0.1$ (this is the model we have previously used to illustrate marginal and extreme multifractal properties). The model fits well the empirical moments $E[\varepsilon_r^q]$ for q up to about 4, but generally gives $K(q)$ values larger than the empirical ones for $q > 4$. The choice or the range of moments to use in fitting the $K(q)$ function is affected by two considerations: (1) the range that is relevant to the rainfall extremes of interest and (2) the accuracy and bias of the empirical values. Concerning the former issue, we know from Eq. 18 that at high resolution (for n very large or equivalently for very small relative durations d/D_{\max}), the return-period values $\varepsilon_{n,T}$ depend only on the values of $K(q)$ in the neighborhood of q_D (here of q_1 , since for temporal rainfall $D = 1$). For the function $K(q)$ given above, $q_1 = 3.2$. For larger relative durations d/D_{\max} , moments of higher order become more important, especially as the return period T increases. While in the limit as $T \rightarrow \infty$ what matters is the behavior of $K(q)$ near q_1^* (in our case $q_1^* = 10$), for combinations of d/D_{\max} and T of typical interest, moments of order larger than about 5 or 6 are not important.

The second consideration in choosing the range of moments is the accuracy and bias of the empirical $K(q)$ values. In this regard one should notice that, as $n \rightarrow \infty$, the return-period value $\varepsilon_{n,T}$ in Eq. 18 is smaller than $cm^{n\gamma}$ for any $c > 0$ and $\gamma > \gamma_1$. This means that, at high resolutions $r = D_{\max}/d$ and in a record of any finite length T , singularities of order $\gamma > \gamma_1$ occur with probability close to 0 and moments $E[\varepsilon_r^q]$ with $q > q_1$ are underestimated with probability close to 1. If one uses the moments of ε_r at small resolutions r , the probability of moment underestimation decreases, but statistical variability increases. All this means that one should fit $K(q)$ models using moments of order not much greater than q_1 . This is an important consideration, since fitting $K(q)$ to moments much higher than q_1 would lead to almost-sure underestimation of the extremes. For a rigorous discussion of this problem, see *Ossiander and Waymire* (2000, 2002). A related phenomenon is the linearization of the empirical $K(q)$ function, as for example discussed in *Lashermes et al.* (2004).

Interestingly, the moment-scaling function $K(q) = 0.1(q^2 - q)$ fits well the empirical moments of rainfall intensity irrespective of season, storm intensity I_b , and storm duration D_{\max} . This makes the interior process independent of the exterior process and suggests that the dynamics responsible for scale invariance in rainfall may have universal characteristics.

Figure 8 shows how the exterior process of Model 1 was fitted using storm duration and intensity data. The empirical rate of storms of duration $D_{\max} \geq 5$ min is $\lambda = 170.5$ storms/year (this reduces to 94 storms/year for storms with duration in excess of 1 hour). The inset of Figure 8a shows that D_{\max} may be assumed to have a three-parameter gamma distribution. We have also found that the upper tail of the conditional storm intensities ($I | D_{\max}$) has lognormal shape. For example, Figure 8b shows the normal distribution fitted by maximum-likelihood to the upper

25% of the $\ln(I|D_{\max})$ data for D_{\max} in the range [35-55] minutes. Notice that the empirical distribution of $\ln(I|D_{\max})$ deviates significantly from a normal distribution in the body and lower tail, but not the upper tail, which is what matters for extreme analysis. This tail-fitting operation has been repeated for different D_{\max} bins, producing the values of $m_{\ln(I|D_{\max})}$ and $\sigma_{\ln(I|D_{\max})}^2$ shown as solid squares and circles in Figure 8a. The lines in the same figure are smooth parametric fits. Finally, $m_{\ln(I|D_{\max})}$ and $\sigma_{\ln(I|D_{\max})}^2$ have been corrected for the effect of dressing, to produce the bare intensity parameters $m_{\ln(I_b|D_{\max})}$ and $\sigma_{\ln(I_b|D_{\max})}^2$ (details of the correction are omitted).

Next we consider parameter estimation for Model 2. For the interior process, the estimation method is simpler than for Model 1, because one does not have to contend with storms of different duration and intensity. In fact, for Model 2 one can proceed as usual and evaluate the moment-scaling properties of the dressed densities for various averaging durations $d < D_{\max}$. Since the record includes dry inter-storm periods, a good fit is obtained using an *sss* model of the beta-lognormal type, with $K(q) = c_{\beta}q + c_{LN}(q^2 - q)$. The parameters (c_{β}, c_{LN}) are estimated to be (0.5, 0.047).

For the exterior process of Model 2, one must estimate D_{\max} as the outer limit of multifractality and the distribution of the bare intensity I_b for intervals of duration D_{\max} . This should be done so that the upper tail or upper moments of the dressed density $I = I_b Z$ for duration D_{\max} match the corresponding tail or moments of the empirical distribution.

We have assumed that I_b has lognormal distribution with some parameters m_{I_b} and $\sigma_{I_b}^2$, and replaced the exact distribution of Z with the distribution of the random scaling factor A_{r_Z} ,

where $r_Z = 2.237$ is chosen to match the exact second-moment of Z as explained in Section 3.3(c). The implication is that the dressed density I has a three-parameter “beta-lognormal” distribution, meaning that the distribution has some probability mass P_o at $I = 0$ (this is the same as the probability that $Z = 0$, which equals 0.45) and $(I|I > 0)$ has lognormal distribution. One can find the parameters $(D_{\max}, m_{I_b}, \sigma_{I_b}^2)$ to either reproduce three empirical moments of I (we have used the moments of order 0, 2 and 4) or reproduce the moment of order 0 and provide a maximum-likelihood fit to the upper tail of the empirical distribution (we have used the upper 25% of the empirical values). The latter procedure gives $D_{\max} = 3.38$ days, $m_{I_b} = 0.187$ mm/h and $\sigma_{I_b}^2 = 0.0251 \text{ mm}^2 / \text{h}^2$. Similar estimates are found when matching the moments.

For Model 3, one may select I_b to be the mean historical rainfall intensity and estimate D_{\max} such that $I_b Z$ reproduces a high moment of the empirical distribution of I . We have chosen to match the third moment. Since now I_b is deterministic, one obtains a larger value of D_{\max} than for Model 2 ($D_{\max} = 14.6$ days). The interior process of Model 3 is practically identical to that of Model 2.

4.3 IDF Curves

Let $\varepsilon_{d,\max}$ be the maximum rainfall intensity in d inside one D_{\max} interval. In any of the above models, the conditional distribution of $\varepsilon_{d,\max}|D_{\max}, I_b$ can be found using the methods of Section 3.3. For example, when using the independent approximation in Eq. 25, the distribution of $\log(\varepsilon_{d,\max}|D_{\max}, I_b)$ is found as

$$F_{\log(\varepsilon_{d,\max}|D_{\max}, I_b)}(\log(\varepsilon)) \approx \begin{cases} [F_{\log(Z)} * f_{\log(A_r)}(\log(\varepsilon/I_b))]^r, & r \geq 1 \\ F_{\log(Z)}(\log(\varepsilon/rI_b)), & r < 1 \end{cases} \quad (26)$$

where $r = D_{\max} / d$.

Notice that the intensity I_b is random for Models 1 and 2 and the duration D_{\max} is random for Model 1, whereas for Model 3 both quantities are deterministic. Hence the unconditional distribution of $\log(\varepsilon_{d,\max})$ for Models 1 and 2 is obtained by taking expectation of the distribution in Eq. 26 with respect to I_b and/or D_{\max} . For example, for Model 1,

$$F_{\log(\varepsilon_{d,\max})}(\log(\varepsilon)) = E_{D_{\max}, I_b} [F_{\log(\varepsilon_{d,\max}|D_{\max}, I_b)}(\log(\varepsilon))] \quad (27)$$

Finally, the IDF value $\varepsilon_{d,T}$ is the value exceeded by $\varepsilon_{d,\max}$ with probability $1/\lambda T$ for Model 1 and with probability D_{\max}/T for Models 2 and 3.

Figure 9 compares model-generated IDF curves (dashed lines) with the empirical IDF curves for Florence (solid lines), using the three models. The model-generated curves have return periods $T = 2, 4, 8, 23, 10^2, 10^3$ and 10^4 years and the empirical curves are for $T = 2, 4, 8$ and 23 years, both increasing from below.

All models produce IDF curves that are generally consistent with the empirical ones and provide similar extrapolations for return periods T longer than the duration of the historical record. Rather small differences can be noted for short averaging durations as well as very long durations. These will be commented upon in an upcoming publication, where issues of statistical variability and seasonal variation will also be addressed. When the model-based IDF curves are compared with the average rainfall intensities from the November 1966 event, one concludes that for d larger than about 1 day that event has a return period of several centuries. This is in general agreement with the historical flood record for the city of Florence (*Becchi and Giuli, 1987*).

5. Conclusions

Significant work has been done over the past two decades to establish the multifractal properties of rainfall in space and time, develop suitable models, and use the models to predict rainfall extremes. This paper is an attempt at presenting the main results in a unified way.

Unfortunately the terminology, notation and analysis of multifractal processes are not standardized. We have argued that an attractive and general definition of multifractality is as a scale-invariance property that extends the classic notion of self-similarity. All the results presented here are consistently derived from this definition. These include marginal and extreme distributions and asymptotic scaling properties of the intensity-duration-frequency (IDF) curves and the areal reduction factor (ARF).

Two important trends underlie the recent work on multifractal rainfall modeling and extreme analysis. One is the shift of focus from the asymptotic scaling relations satisfied by the IDF curves and the ARF to the calculation of exact extreme distributions of time and time-space averages under non-asymptotic conditions. The latter distributions are the results needed for many hydrologic applications.

The second trend is a more sparing use of multifractality in rainfall modeling, which recognizes the limits of scale invariance in space-time rainfall. This trend is producing models that are more consistent with rainfall records, again making the results more suitable for application. The fact that rainfall is not a simple multifractal process increases the complexity of the models, but we have shown that to evaluate rainfall extremes even rough models suffice, provided one estimates the parameters to reproduce an appropriate range of empirical moments or upper-tail statistics.

While the use of scale-invariance in rainfall modeling has come of age and a consistent theory of extremes using these models has emerged, some questions and needs still remain to be addressed. On the one hand there is the practical need to make the theory more user-friendly and relevant for application. For example, issues of robustness, validation, and regionalization should be addressed before multifractal models are routinely used to assess extreme precipitation. A

systematic study to identify best-performing rainfall models, balancing accuracy with simplicity and robustness, should also be made.

On the theoretical side, one needs to better understand the sources of multifractality in rainfall. The link to turbulent convection should be explored in greater depth to determine the extent to which turbulence really affects rainfall scaling. The complex cloud processes that lead to condensation, coalescence and ultimately precipitation should be analyzed to provide a better theoretical underpinning of the relationship between the properties of atmospheric convection and rainfall, shed light on the universality (or lack thereof) of the scaling parameters under stratiform, convective and other conditions, and assess the effects of various fluid-dynamics and microphysical processes at different scales.

Acknowledgments

This work was supported in part by the National Science Foundation under Grant No. EAR-0228835, in part by the Alexander S. Onassis Public Benefit Foundation under Scholarship No. F-ZA 054/2005-2006, and in part by the MURST ex 60% 60ROSS05 Fund of the University of Salerno. The authors acknowledge the useful comments and suggestions of two reviewers.

Appendix A: Derivation of the Large-deviation Result in Eq. 14

What follows extends the derivation of the “rough” relationship $P[\varepsilon_{r,b} > r^\gamma] \sim r^{-C_b(\gamma)}$ given in *Schertzer and Lovejoy* (1996), pp. 55-56. The extension produces the function $g_b(r, \gamma)$ in Eq. 14, in addition to $C_b(\gamma)$. The analysis is for bare cascades, but to simplify the notation we drop the subscript b .

We know that

$$E[\varepsilon_r^q] = r^{K(q)} \quad (\text{A1})$$

and write the distribution of ε_r as

$$1 - F_{\varepsilon_r}(r^\gamma) = g(r, \gamma) r^{-C(\gamma)} \quad (\text{A2})$$

We determine the asymptotic functions $g(r, \gamma)$ and $C(\gamma)$ as $r \rightarrow \infty$ by recovering Eq. A1 from Eq. A2, using the saddle-point approximation to integrals of the type $I(\xi) = \int_{x_1}^{x_2} g(x) e^{\xi f(x)} dx$,

where the function $f(x)$ has a maximum and is twice differentiable at a point x_m , $x_1 < x_m < x_2$.

The approximation is obtained by expanding $f(x)$ in Taylor series around x_m , as

$$f(x) = f(x_m) - \frac{1}{2} |f''(x_m)| (x - x_m)^2 + \dots \text{ This gives,}$$

$$I(\xi) = g(x_m) e^{\xi f(x_m)} \int_{x_1}^{x_2} \frac{g(x)}{g(x_m)} e^{-\frac{1}{2} \xi |f''(x_m)| (x - x_m)^2} dx \quad (\text{A3})$$

For large ξ , the integral approaches $\left(\frac{2\pi}{\xi |f''(x_m)|} \right)^{1/2}$ and $I(\xi)$ approaches

$$I(\xi) \approx g(x_m) e^{\xi f(x_m)} \left(\frac{2\pi}{\xi |f''(x_m)|} \right)^{1/2} \quad (\text{A4})$$

Now consider the moments $E[\varepsilon_r^q] = \int f_{\varepsilon_r}(\varepsilon) \varepsilon^q d\varepsilon$ in Eq. A1. For given r , we put $\varepsilon = r^\gamma$ and use $f_\varepsilon d\varepsilon = f_\gamma d\gamma$ to write these moments as

$$E[\varepsilon_r^q] = \int f_\gamma(\gamma) r^{q\gamma} d\gamma \quad (\text{A5})$$

It follows from Eq. A2 that $\gamma = \log_r(\varepsilon_r)$ has distribution $1 - F_\gamma(\gamma) = g(r, \gamma) r^{-C(\gamma)}$. Therefore

$$\begin{aligned} f_\gamma(\gamma) &= \left[-\frac{\partial g(r, \gamma)}{\partial \gamma} + \ln(r) C'(\gamma) g(r, \gamma) \right] r^{-C(\gamma)} \\ &\approx \ln(r) C'(\gamma) g(r, \gamma) r^{-C(\gamma)} \end{aligned} \quad (\text{A6})$$

As $r \rightarrow \infty$, the term $\frac{\partial g(r, \gamma)}{\partial \gamma}$ becomes negligible relative to $\ln(r)C'(\gamma)g(r, \gamma)$ (see below);

this is why in Eq. A6 this term was neglected. Substitution of Eq. A6 into Eq. A5 gives

$$E[\varepsilon_r^q] = \ln(r) \int C'(\gamma)g(r, \gamma)e^{\ln(r)[q\gamma - C(\gamma)]} d\gamma \quad (\text{A7})$$

For $\ln(r)$ large, we can use the saddle-point approximation in Eq. A4 to obtain

$$E[\varepsilon_r^q] = \ln(r) [C'(\gamma)g(r, \gamma)]_{\gamma(q)} \left(\frac{2\pi}{\ln(r) |C''(\gamma(q))|} \right)^{1/2} r^{\gamma(q)} \quad (\text{A8})$$

where $\gamma(q)$ is the value of γ that maximizes $[q\gamma - C(\gamma)]$. In order for $E[\varepsilon_r^q]$ in Eq. A8 to equal $\lambda^{K(q)}$, it must be

$$K(q) = \max_{\gamma} [q\gamma - C(\gamma)] \quad (\text{A9})$$

and

$$\ln(r) [C'(\gamma)g(r, \gamma)]_{\gamma(q)} \left(\frac{2\pi}{\ln(r) |C''(\gamma(q))|} \right)^{1/2} = 1 \quad (\text{A10})$$

From Eq. A10,

$$g(r, \gamma) = \left[2\pi \frac{(C'(\gamma))^2}{C''(\gamma)} \ln(r) \right]^{-1/2} \quad (\text{A11})$$

To determine whether $\frac{\partial g(r, \gamma)}{\partial \gamma}$ is negligible relative to $\ln(r)C'(\gamma)g(r, \gamma)$, as assumed in Eq.

A6, one can evaluate the derivative of $g(r, \gamma)$ in Eq. A11. This gives

$$-\frac{\partial g(r, \gamma)}{\partial \gamma} = \pi \ln(r) \left[2\pi \frac{(C'(\gamma))^2}{C''(\gamma)} \ln(r) \right]^{-3/2} d \left(\frac{(C'(\gamma))^2}{C''(\gamma)} \right) \frac{1}{d\gamma} \quad (\text{A12})$$

and the ratio

$$\frac{-\frac{\partial g(r, \gamma)}{\partial \gamma}}{\ln(r)C'(\gamma)g(r, \gamma)} = \frac{\pi}{C'(\gamma)} \left[2\pi \frac{(C'(\gamma))^2}{C''(\gamma)} \ln(r) \right]^{-1} d \left(\frac{(C'(\gamma))^2}{C''(\gamma)} \right) \quad (\text{A13})$$

For $r \rightarrow \infty$, the ratio in Eq. A13 tends to 0, justifying the asymptotic expression in Eq. A11.

Appendix B: Derivation of the Critical Moment Order q_D^*

At level $n + 1$, each cascade tile Ω_n is partitioned into m^D tiles $\Omega_{n+1,i}$. Hence the sss scaling

property $\varepsilon_{n+1} = A_m \varepsilon_n$ may be written as $\varepsilon_{n+1} = A_m \frac{1}{m^D} \sum_{i=1}^{m^D} \varepsilon_{n+1,i}$ where $\varepsilon_{n+1,i}$ is the dressed

density in $\Omega_{n+1,i}$. If $E[\varepsilon_{n+1}^q]$ exists, then using $E[A_m^q] = m^{K_b(q)}$ from Eq. 5 gives

$$E[\varepsilon_{n+1}^q] = m^{K_b(q)} \frac{1}{m^{qD}} E\left[\left(\sum_{i=1}^{m^D} \varepsilon_{n+1,i}\right)^q\right] \quad (\text{B1})$$

Since $\varepsilon_{n+1,i} \geq 0$ with $P[\varepsilon_{n+1,i} > 0] > 0$ (due to non-degeneracy) and $q > 1$, the expectation on the right hand side of Eq. B1 is bounded from below by $m^D E[\varepsilon_{n+1}^q]$, giving

$$E[\varepsilon_{n+1}^q] > m^{K_b(q)} \frac{1}{m^{qD}} m^D E[\varepsilon_{n+1}^q] \quad (\text{B2})$$

One concludes that existence of $E[\varepsilon_{n+1}^q]$ implies $K_b(q) < D(q - 1)$. Since $K(q) = K_b(q)$ whenever $E[\varepsilon_{n+1}^q]$ exists, it must also be $K(q) < D(q - 1)$. This derivation applies not just to discrete cascades, but in general to all stationary sss measures.

Appendix C: Asymptotic Scaling of Return-period Values

We use Eq. 13 to obtain the asymptotic behavior of $\varepsilon_{n,T}$ for ($n \rightarrow \infty$, T finite) and (n finite,

$T \rightarrow \infty$). In either case, the level $m^{n\gamma}$ in Eq. 13 diverges and the function $g(m^n, \gamma)$ in Eq. 16,

which varies slowly with m^n , becomes immaterial to the scaling of $\varepsilon_{n,T}$. Therefore one can study the asymptotic scaling properties of $\varepsilon_{n,T}$ using the rougher, large- m^n relations

$$P[\varepsilon_n \geq m^{n\gamma}] \sim m^{-nC(\gamma)} = \begin{cases} m^{-nC_b(\gamma)}, & \gamma < \gamma_D^* \\ m^{-n[q_D^*\gamma - D(q_D^* - 1)]}, & \gamma > \gamma_D^* \end{cases} \quad (\text{C1})$$

where we have used Eq. 15 for $C(\gamma)$. The objective is to find γ such that

$$m^{-nC(\gamma)} = \frac{1}{m^{nD}T} = m^{-n(D + \log_{m^n} T)}, \text{ hence such that } C(\gamma) = D + \log_{m^n}(T).$$

Consider first the high-resolution limit when $n \rightarrow \infty$ while T is finite. As shown below, in this case $\gamma < \gamma_D^*$. Therefore $C(\gamma) = C_b(\gamma)$ and γ must satisfy $C_b(\gamma) = D + \log_{m^n}(T)$. Notice that, for T finite, $\log_{m^n}(T) \rightarrow 0$ as $n \rightarrow \infty$. Hence γ is infinitesimally close to the value γ_D such that $C_b(\gamma_D) = D$ and one may use linear Taylor series expansion of $C_b(\gamma)$ around γ_D . The expansion is $C_b(\gamma) = D + q_D(\gamma - \gamma_D)$, where $q_D = C_b'(\gamma_D)$ is the moment order associated with γ_D . Solving $D + q_D(\gamma - \gamma_D) = D + \log_{m^n}(T)$ for γ gives $\gamma = \gamma_D + \frac{1}{q_D} \log_{m^n}(T)$. We conclude that, under ($n \rightarrow \infty$, T finite), the return-period value $\varepsilon_{n,T} = m^{n\gamma}$ scales with m^n and T as

$$\varepsilon_{n,T} \sim m^{n\gamma_D} T^{1/q_D} \quad (\text{C2})$$

Since $\gamma_D < \gamma_D^*$, our previous use of the first expression in Eq. C1 is justified.

Next consider the case when n is finite and $T \rightarrow \infty$. Since m^n is finite and $m^{n\gamma} \rightarrow \infty$, it must be $\gamma \rightarrow \infty$ and one must use the expression in Eq. C1 for $\gamma > \gamma_D^*$. The condition

$$q_D^*\gamma - D(q_D^* - 1) = D + \log_{m^n}(T) \text{ gives } \gamma = D + \frac{1}{q_D^*} \log_{m^n}(T) \text{ and}$$

$$\varepsilon(n,T) \approx m^{nD} T^{1/q_D^*} \quad (\text{C3})$$

The following generalization of the previous problem is needed for space-time rainfall extremes. As before, we consider the dressed densities $\varepsilon_{n,i} = \varepsilon(\Omega_{n,i})$, but now seek the extremes of $\varepsilon_{n,i}$ over the tiles $\Omega_{n,i}$ of Ω_0 with centerpoint in a D' -dimensional subspace, $1 \leq D' \leq D$. For example, in the case of space-time rainfall, $D = 3$ but one is interested in the maximum of space-time averages over time only ($D' = 1$), not over time and space ($D' = 3$).

In this more general setting, $\varepsilon_{n,T}$ is the value exceeded by ε_n with probability $1/(m^{nD'}T)$. Therefore γ must be such that $C(\gamma) = D' + \log_{m^n}(T)$. Following step by step the previous analysis one finds

$$\varepsilon_{n,T} \sim \begin{cases} m^{n\gamma_{D'}} T^{1/q_{D'}}, & \text{for } n \rightarrow \infty, T \text{ finite} \\ m^{n[D-(D-D')/q_D^*]} T^{1/q_D^*}, & \text{for } n \text{ finite}, T \rightarrow \infty \end{cases} \quad (\text{C4})$$

List of symbols

a : averaging area

a_r : deterministic *sss* amplitude scaling factor for a scale change factor r

A_r : random *sss* amplitude scaling factor for a scale change factor r

c_{LN} : lognormal co-dimension coefficient

c_{sss} (d_{sss}): *sss* under contraction (under dilation)

c_β : beta co-dimension coefficient

$C(\gamma)$: co-dimension function of dressed cascade

$C_b(\gamma)$: co-dimension function of bare cascade

d : averaging duration

D : embedding Euclidean dimension

$D(\gamma)$: fractal dimension of singularities of order γ
 D_{\max} : outer limit of multifractality in time (= storm duration in Sec. 4)
 I : dressed mean storm intensity
 I_b : bare mean storm intensity
 $K(q)$: $K(q)$ for dressed cascades
 $K_b(q)$: $K(q)$ for bare cascades
 l : linear dimension of geographical averaging region
 m : linear cascade multiplicity
 n : cascade level
 $N(r, \gamma)$: number of cubic tiles at resolution r where $\varepsilon_r > r^\gamma$
 q : moment order
 q_D : moment order associated with γ_D
 q_D^* : critical order of moment divergence for a D -dimensional cascade
 r : resolution (also scale-change factor)
 r_Z : scale change factor such that A_{r_Z} matches a given moment of Z
 ss : self-similarity
 sss : stochastic self-similarity
 $S_X(\omega)$: spectral density function of $X(t)$
 T : return period
 $X(t)$: stationary random process in R^D
 $X(\Omega)$: measure of Ω
 Z : dressing factor

γ : singularity exponent

γ_D : singularity exponent that satisfies $C_b(\gamma_D) = D$

γ_D^* : singularity exponent associated with q_D^*

$\mathcal{E}(\Omega)$: average measure density in Ω

$\varepsilon_{d,\max}$: maximum of the average rainfall intensity in d for a storm of duration D_{\max}

$\varepsilon_n = \mathcal{E}(\Omega_n)$: average dressed density in Ω_n

$\varepsilon_{n,b} = \varepsilon_b(\Omega_n)$: bare density in Ω_n

$\varepsilon_{n,\max}$: maximum of the dressed densities $\varepsilon_{n,i} = \mathcal{E}(\Omega_{n,i})$ at cascade level n

$\varepsilon_{n,T}$: value expected to be exceeded once by ε_n in T cascade realizations

ε_{n_s, n_t} : average random measure over a square geographical region of side length l and a time

interval of duration $d = m^{-n_t}$

$\varepsilon_{n_s, n_t, T}$: value expected to be exceeded once by ε_{n_s, n_t} in T space-time cascade realizations

$1/m^{-n_s D}$

ε_r : average measure density in a cube of side length $1/r$

λ : annual rate of storms

$\eta_{n_s, n_t, T}$: areal reduction factor for a square area with linear dimension $l = m^{-n_s}$ and a time

interval of duration $d = m^{-n_t}$

$\underline{\omega}$: frequency vector

Ω_{\max} : largest region inside which the *csss* property holds

Ω_{\min} : smallest region above which the *dsss* property holds

Ω_n : cubic tile at cascade level n

Ω_0 : unit D -dimensional cube

References

- Asquith, W.H. and J. S. Famiglietti (2000), "Precipitation Areal-reduction Factor Estimation Using an Annual-maxima Centered Approach," *J. Hydrol.*, **230**: 55-69.
- Becchi, I. and D. Giuli (1987), "Description of the Arno Project: A Real-time Approach to the Arno River Flooding Forecast," *Proceedings, International Conference on the Arno Project*, National Group for the Prevention of Hydro-geological Disasters, CNR, Tecnoprint, Bologna, pp. 9-49.
- Becchi, I. and F. Castelli (1989), *Lettura e archiviazione digitali di registrazioni pluviografiche ad alta risoluzione temporale*, Technical Report 1/89, Dep. of Civil Eng., University of Firenze, Italy.
- Bell, F.C. (1976), *The Areal Reduction Factors in Rainfall Frequency Estimation*, Rep. No. 35, Institute of Hydrology, Wallingford, U.K.
- Bernard, M. M. (1932), "Formulas for Rainfall Intensities of Long Durations," *Trans. ASCE*, **96**: 592-624.
- Burlando, P. and R. Rosso (1996), "Scaling and Multiscaling Models of Depth-Duration-Frequency Curves for Storm Precipitation," *J. Hydrol.*, **187**: 45-64.
- Castro, J., A. Cârsteanu, and C. Flores (2004), "Intensity-duration-area-frequency Functions for Precipitation in a Multifractal Framework," *Physica A*, **338**(1-2): 206-210.
- Cates, M. E. and J. M. Deutsch (1987), "Spatial Correlations in Multifractals," *Phys. Rev. A*, **35**(11): 4907-4910.

- Chow, V. T., D. R. Maidment, and L. W. Mays (1988), *Applied Hydrology*, McGraw-Hill, New York.
- Cramer, H. (1938), “Sur un nouveau theoreme-limite de la theorie des probabilites,” *Actualites Scientifiques et Industrielles*, No. 736 of Colloque consacre a la theorie des probabilites, pp. 5-23, Herrman, Paris.
- De Michele, C., N. T. Kottegoda, and R. Rosso (2001), “The Derivation of Areal Reduction Factor of Storm Rainfall from Its Scaling Properties,” *Water Resour. Res.*, **37**(12), 3247-3252.
- Deidda, R. (2000), “Rainfall Downscaling in a Space-time Multifractal Framework,” *Water Resour. Res.*, **36**: 1779-1794.
- Deidda, R., M. G. Badas and E. Piga (2004), Space-time scaling in high-intensity Tropical Ocean Global Atmosphere Coupled Ocean-Atmosphere Response Experiment (TOGA-COARE) storms, *Water Res. Res.*, **40**, W02506, doi: 10.1029/2003WR002574.
- Deidda, R., R. Benzi, and F. Siccardi (1999), “Multifractal Modeling of Anomalous Scaling Laws in Rainfall,” *Water Resour. Res.*, **35**: 1853-1867.
- Dembo, A. and O. Zeitouni (1993), *Large Deviations Techniques and Applications*, Jones and Bartlett Publishers, Boston.
- Eagleson, P. S. (1970), *Dynamic Hydrology*, McGraw-Hill, New York.
- Feller, W. (1968), *An Introduction to Probability Theory and Its Applications, Vol. 1*, John Wiley & Sons, New York.

- Fraedrich, K. and C. Larnder (1993), "Scaling Regimes of Composite Rainfall Time Series," *Tellus*, **45A**: 289-298.
- Gupta, V. K. and E. C. Waymire (1990), "Multiscaling Properties of Spatial Rainfall and River Flow Distributions," *J. Geophys. Res.* **95**, 1999-2009.
- Gupta, V.K. and E. C. Waymire (1993), "A Statistical Analysis of Mesoscale Rainfall as a Random Cascade," *J. Appl. Meteorol.*, **32**(2): 251-267.
- Harris, D., M. Menabde, A. Seed, and G. Austin (1998), "Breakdown Coefficients and Scaling Properties of Rain Fields," *Nonlinear Proc. Geophys.*, **5**: 93-104.
- Hubert, P., H. Bendjoudi, D. Schertzer, and S. Lovejoy (1998), "A Multifractal Explanation for Rainfall Intensity-Duration-Frequency Curves," *Proceedings, Int. Conf. On Heavy Rains and Flash Floods, Istanbul, Turkey*.
- Kahane, J.-P., and J. Peyriere (1976), "Sur certaines martingales de Benoit Mandelbrot," *Adv. Math.*, **22**: 131-145.
- Koutsoyiannis, D., D. Kozonis, and A. Manetas (1998), "A Mathematical Framework for Studying Rainfall Intensity-Duration-Frequency Relationships," *J. Hydrol.*, **206**: 118-135.
- Koutsoyiannis, D. and T. Xantopoulos (1999), *Engineering Hydrology* (in Greek), 3th Ed., Dept. of Water Resources, Hydraulic and Maritime Engineering, National Technical University of Athens, Greece.

- Lashermes, B., P. Abry and P. Chainais (2004), New Insights into the Estimation of Scaling Exponents, *Int. Jour. of Wavelets, Multir. and Inf. Proc.*, **2**, 497-523.
- Leclerc, G. and J. C. Schaake (1972) *Derivation of Hydrologic Frequency Curves*, Report 142, Dept. of Civil Engineering, MIT, Cambridge, Mass.
- Lovejoy, S. and D. Schertzer (1995), "Multifractals and Rain," in A.W. Kundzewicz (ed.), *Uncertainty Concepts in Hydrology and Hydrological Modelling*, Cambridge Press, 62-103.
- Mandelbrot, B. B. (1974), "Intermittent Turbulence in Self-similar Cascades: Divergence of High Moments and Dimension of the Carrier," *J. Fluid Mech.*, **62**(2): 331-358.
- Marsan, D., D. Schertzer, and S. Lovejoy (1996), "Causal Space-time Multifractal Processes: Predictability and Forecasting of Rain Fields," *J. Geophys. Res.*, **101**(D21): 26,333-26,346.
- Menabde, M, Harris, D., Seed, A., Austin, G and Stow, D. (1997), "Multiscaling Properties of Rainfall and Bounded Random Cascades," *Wat. Res. Res.*, **33**(12): 2823-2830.
- Menabde, M. and Sivapalan, M. (2000), "Modeling of Rainfall Time Series and Extremes Using Bounded Random Cascades and Levy-stable Distributions," *Wat. Res. Res.*, **36**(11): 3293-3300.
- Natural Environmental Research Council (NERC) (1975), *Flood Studies report*, Vol. 2, Institute of Hydrology, Wallingford, U.K.

- O'Neil, J. and C. Meneveau (1993), "Spatial Correlations in Turbulence: Predictions from the Multifractal Formalism and Comparison with Experiments." *Phys. Fluid A*, **5**(1): 158-172.
- Olsson, J., (1995), "Limits and Characteristics of the Multifractal Behavior of a High-Resolution Rainfall Time Series," *Nonlinear Processes in Geophysics*, **2**: 23-29.
- Olsson, J., J. Niemczynowicz, and R. Berdtsson (1993), "Fractal Analysis of High-resolution Rainfall Time-series," *J. Geophys. Res.*, **98**(D12): 23,265-23,274.
- Ossiander, M. and E. C. Waymire (2000), Statistical Estimation for Multiplicative Cascades, *Ann. Statist.*, **28**, 1533-1560.
- Ossiander, M. and E. C. Waymire (2002), On Estimation Theory for Multiplicative Cascades, *The Indian Journal of Statistics*, **64**, 323-343
- Over, T. M. and V. K. Gupta (1996), "A Space-time Theory of Mesoscale Rainfall Using Random Cascades," *J. Geophys. Res.* **101**: 26,319-26,331.
- Parisi, G. and U. Frisch (1985), "On the Singularity Structure of Fully Developed Turbulence," in *Turbulence and Predictability in Geophysical Fluid Dynamics*, edited by M. Ghil, R. Benzi and G. Parisi, North-Holland, Amsterdam.
- Samorodnitsky, G. and M. S. Taqqu (1994), *Stable Non-Gaussian Random Processes*, Chapman & Hall, New York.
- Schertzer, D. and S. Lovejoy (1991), "Nonlinear Geodynamical Variability: Multiple Singularities, Universality and Observables," in D. Schertzer and S. Lovejoy (eds.),

NonLinear Variability in Geophysics, Kluwer Academic Publishers, The Netherlands, pp. 41-82.

Schertzer, D. and S. Lovejoy (1987), "Physical Modeling and Analysis of Rain and Clouds by Anisotropic Scaling of Multiplicative Processes," *J. Geophys. Res.*, **92**: 9693-9714.

Schertzer, D. and S. Lovejoy (1996), *Resolution Dependence and Multifractals in Remote Sensing and Geophysical Information Systems*, Lecture Notes, McGill University, Montreal.

Sherman, C. W. (1931), "Frequency and Intensity of Excessive Rainfall at Boston," *Trans. ASCE*, **95**:951-960.

Schmitt, F., Vannistem, S. and A. Barbosa (1998), "Modeling of Rainfall Time Series Using Two-state Renewal Processes and Multifractals," *J. Geophys. Res.*, **103 (D18)**: 23,181-23,193.

Sivapalan, M. and G. Blöschl (1998), "Transformation of point rainfall: Intensity-duration-frequency curves," *Journal of Hydrology*, **204**: 150-167.

Varadhan, S. R. S. (1984), *Large Deviations and Applications*, Society for Industrial and Applied Mathematics, Philadelphia.

Veneziano, D. (1999), "Basic Properties and Characterization of Stochastically Self-Similar Processes in R^D ," *Fractals*, **7(1)**: 59-78.

Veneziano, D. (2002), "Large Deviations of Multifractal Measures," *Fractals*, **10**: 117-129.
Erratum in *Fractals*, **13(2)**: 1-3 (2005).

- Veneziano, D. and P. Furcolo (2002a), "Multifractality of Rainfall and Intensity-duration-frequency Curves," *Wat. Resour. Res.*, **38**(12): 1306-1317.
- Veneziano, D. and Furcolo, P. (2002b), "Scaling of Multifractal Measures under Affine Transformations," *Fractals*, **10**(2), 147-156.
- Veneziano, D. and P. Furcolo (2003), "Marginal Distribution of Stationary Multifractal Measures and Their Haar Wavelet Coefficients," *Fractals*, **11**(3): 253-270.
- Veneziano, D. and V. Iacobellis (2002), "Multi-scaling Pulse Representation of Temporal Rainfall," *Water Resour. Res.* **38**: 13-1/13.
- Veneziano, D. and A. Langousis (2005a), "The Areal Reduction Factor: A Multifractal Analysis," *Water Resour. Res.*, 41, W07008.
- Veneziano, D. and A. Langousis (2005b), "The Maximum of Multifractal Cascades: Exact Distribution and Approximations," *Fractals*, **13**(4): 1-14.
- Venugopal, V., E. Foufoula-Georgiou, and V. Sapozhnikov (1999a), "A Space-time Downscaling Model for Rainfall," *J. Geophys. Res.*, **104**(D16): 19,705-19,721.
- Venugopal, V., E. Foufoula-Georgiou, and V. Sapozhnikov (1999b), "Evidence of Dynamic Scaling in Space-time Rainfall," *J. Geophys. Res.*, **104**(D24): 31,599-31,610.
- Willems, P. (2000), "Compound Intensity/Duration/Frequency Relationships of Extreme Precipitation for Two Seasons and Two Storm Types," *J. Hydrol.*, **233**: 189-205.

Wilson, J., D. Schertzer and S. Lovejoy (1991), “Continuous Multifractal Cascade Models of Rain and Clouds,” in D. Schertzer and S. Lovejoy (eds.), *NonLinear Variability in Geophysics*, Kluwer Academic Publishers, The Netherlands, pp. 185-207.

Yaglom, A. M. (1986), *Correlation Theory of Stationary and Related Random Functions, Vol. 1, Basic Results*, Springer-Verlag, New York.

Figure Captions

Figure 1: (a) Partition of the unit cube into cascade tiles at different levels n for the case when $D = 2$ and $m = 2$; (b) simulated realization of a stationary *sss* measure density on the plane.

Figure 2: Illustration of the moment scaling function $K(q)$ and co-dimension function $C(\gamma)$. The moment orders q_D and q_D^* and the “singularity orders” γ_D and γ_D^* are relevant to multifractal extremes.

Figure 3: Consecutive approximations to the probability density function of Z for a binary cascade ($m = 2$) on the line ($D = 1$), with moment scaling function $K(q) = 0.1(q^2 - q)$. Calculation was stopped at iteration 26, when a convergence criterion was met. The inset shows the moment ratio $E[Z^q]/E[(Z^{(26)})^q]$ for $q = 1, 2, \dots, 9$ (moments of order 10 or greater diverge).

Figure 4: Return-period values $\varepsilon_{n,T}$ for a multifractal cascade with moment scaling function $K(q) = 0.1(q^2 - q)$. The plots show $\varepsilon_{n,T}$ against the averaging duration $d = m^{-n}$ for $T = 10, 10^2, 10^3, 10^4, 10^5$ and 10^6 cascade realizations (T increases from bottom to top).

Figure 5: Idealization of rainfall as a discrete cascade inside the unit cube in (x,y,t) -space, with moment scaling function $K(q) = 0.1(q^2 - q)$. (a) Dependence of the areal reduction factor ARF on the side length l of the square averaging region and the duration d of temporal averaging. (b) Scaling of the ARF factor with the ratio l/d . For large l/d ratios, the ARF behaves like a power function of l/d , with exponent $-\gamma_1 = -0.532$.

Figure 6: Return-period values $\varepsilon_{n,T}$ for the multifractal cascade used in Figure 4: (a) exact values using the distribution of $\varepsilon_{n,\max}$, (b) approximation when Z is replaced with A_{rZ}

using a second-moment matching criterion ($r_Z = 2.237$), and (c) approximation when, in addition, one neglects dependence among the cascade tiles. Return periods are $T = 10, 10^2, 10^3, 10^4, 10^5$ and 10^6 cascade realizations, increasing from bottom to top.

Figure 7: Schematic representation of the “exterior process” for rainfall models 1, 2, and 3. In all cases, the interior process is stationary multifractal with independent realizations inside different D_{\max} intervals.

Figure 8: Use of Model 1 to evaluate the IDF curves for Florence, Italy, based on a 23-year record: (a) Fitted gamma distribution of storm duration D_{\max} (inset) and mean and variance of the conditional log storm intensity ($\ln I | D_{\max}$). (b) Example tail fit by maximum-likelihood of a normal distribution to $\ln(I)$ for D_{\max} between 35 and 55 minutes.

Figure 9: Comparison of model-generated IDF curves (dashed lines) and empirical IDF curves (solid lines) for Florence, Italy, using rainfall models 1, 2 and 3. The model-generated curves are for return periods $T = 2, 4, 8, 23, 10^2, 10^3$ and 10^4 years and the empirical curves are for $T = 2, 4, 8$ and 23 years, both increasing from below.

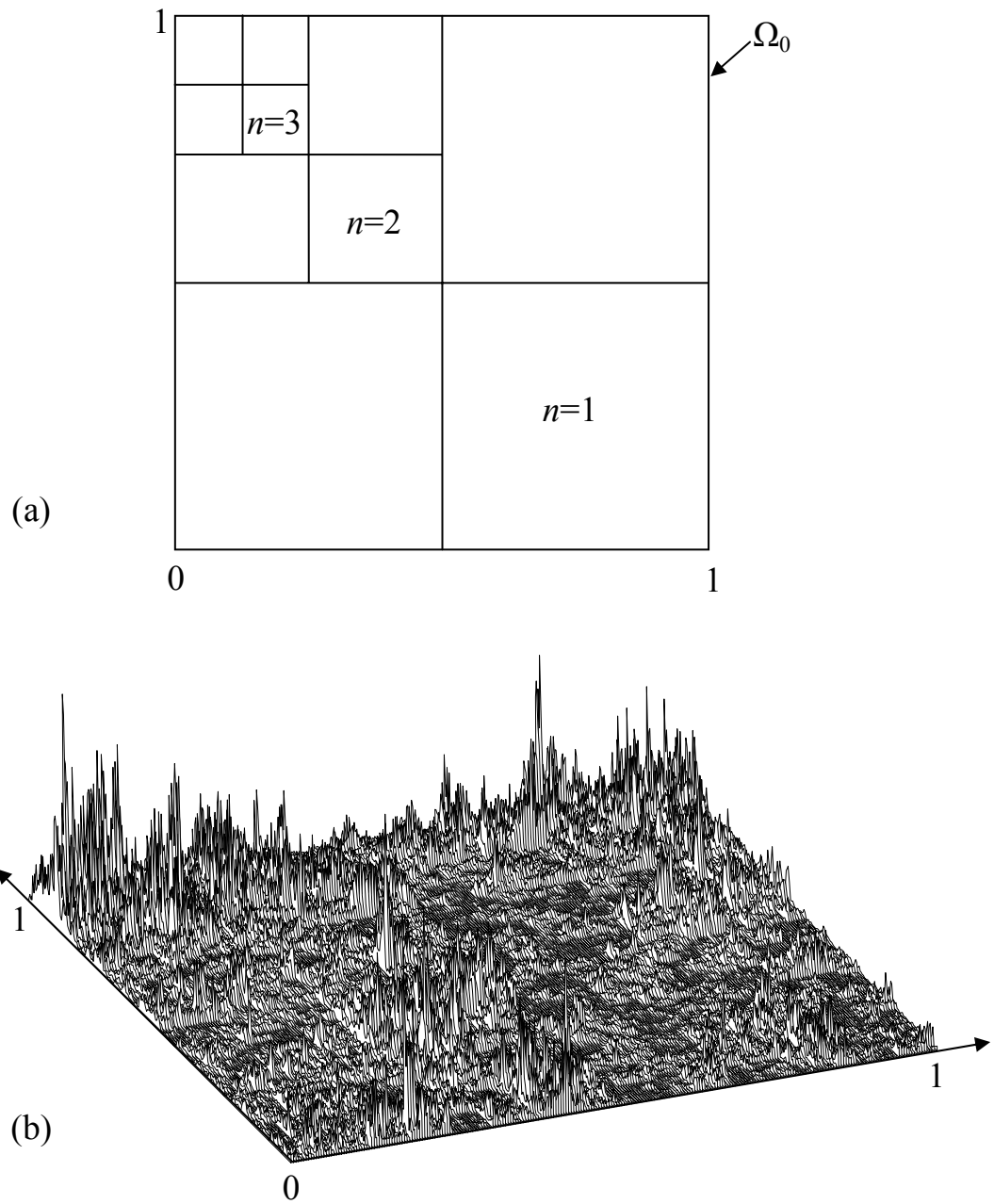


Figure 1: (a) Partition of the unit cube into cascade tiles at different levels n for the case when $D = 2$ and $m = 2$; (b) simulated realization of a stationary sss measure density on the plane.

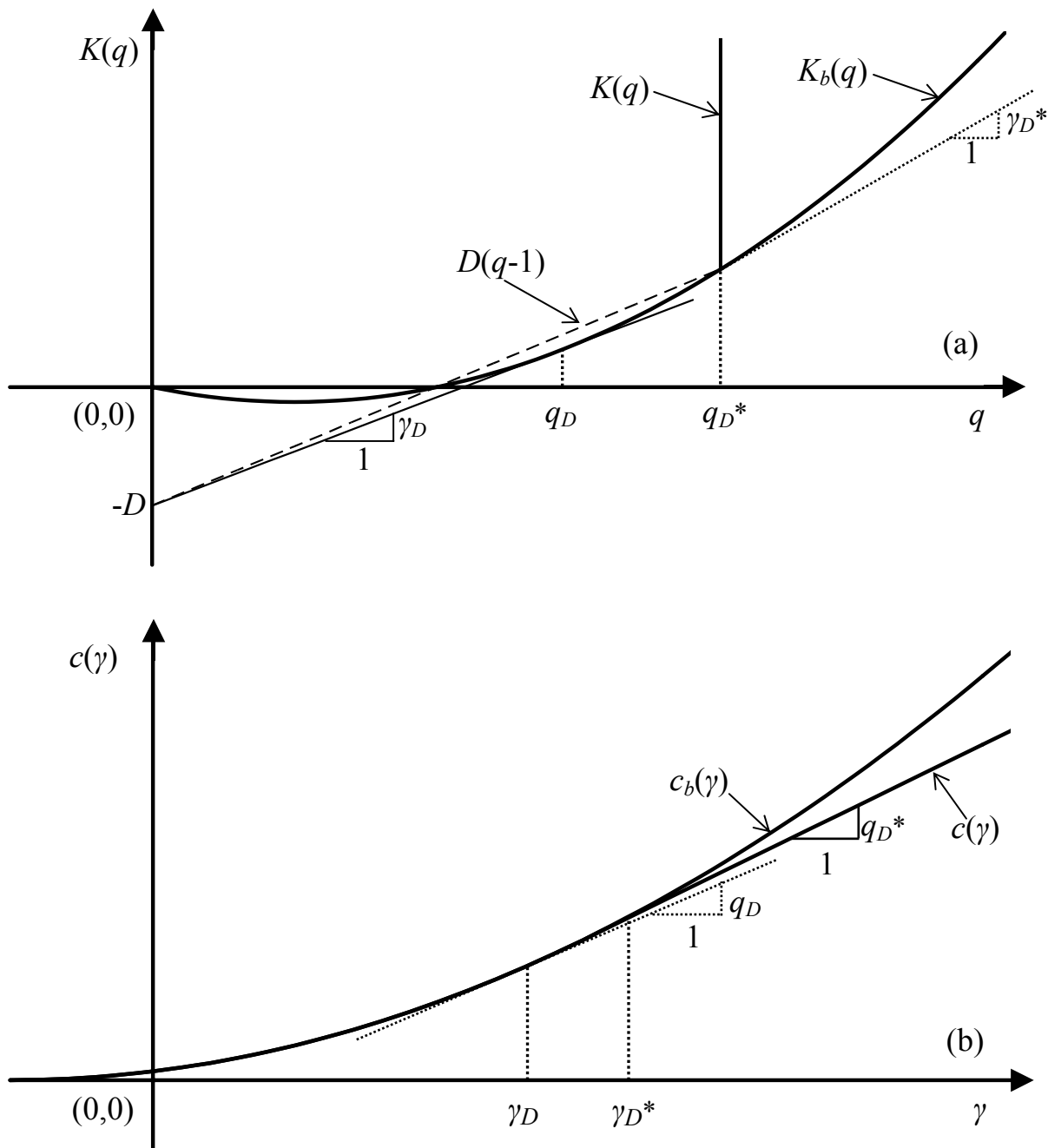


Figure 2: Illustration of the moment scaling function $K(q)$ and co-dimension function $C(\gamma)$. The moment orders q_D and q_D^* and the “singularity orders” γ_D and γ_D^* are relevant to multifractal extremes.

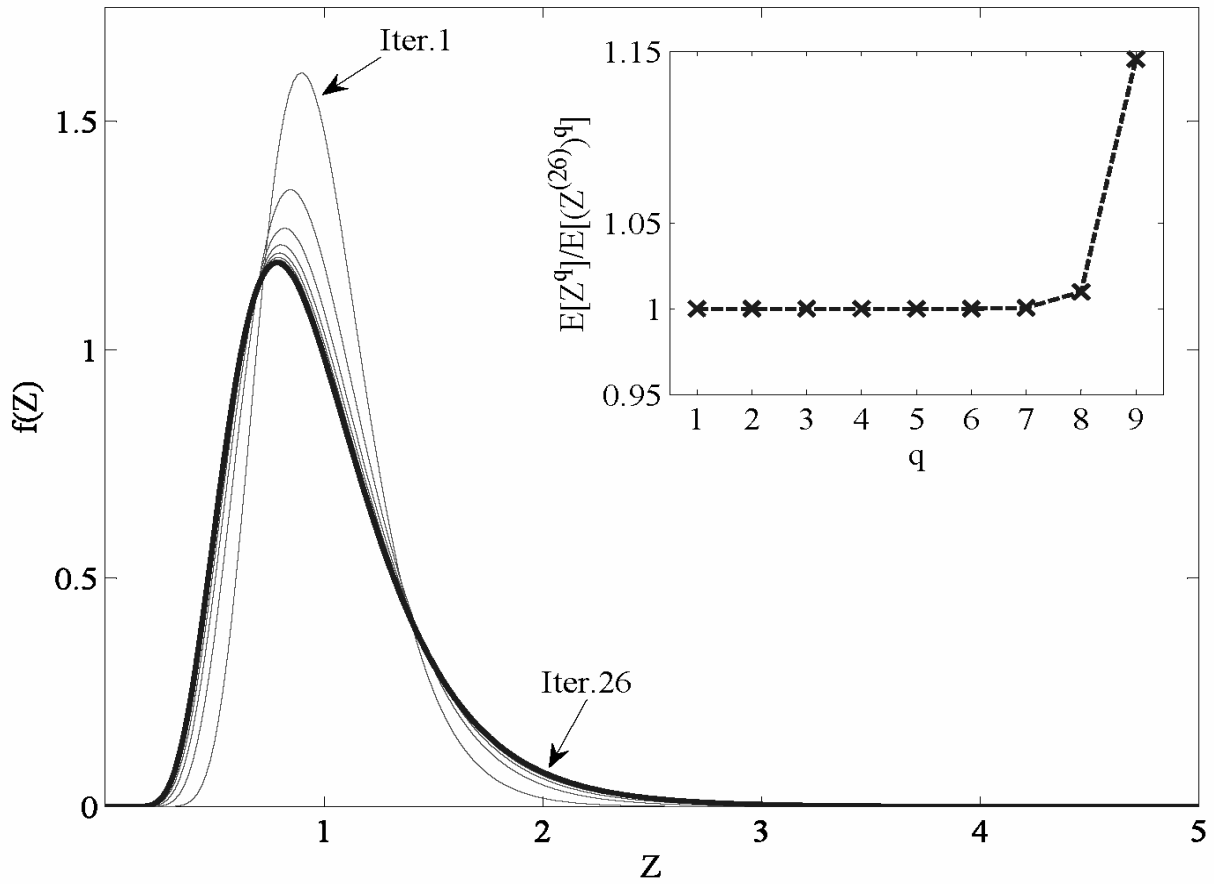


Figure 3: Consecutive approximations to the probability density function of Z for a binary cascade ($m = 2$) on the line ($D = 1$), with moment scaling function $K(q) = 0.1(q^2 - q)$. Calculation was stopped at iteration 26, when a convergence criterion was met. The inset shows the moment ratio $E[Z^q]/E[(Z^{(26)})^q]$ for $q = 1, 2, \dots, 9$ (moments of order 10 or greater diverge).

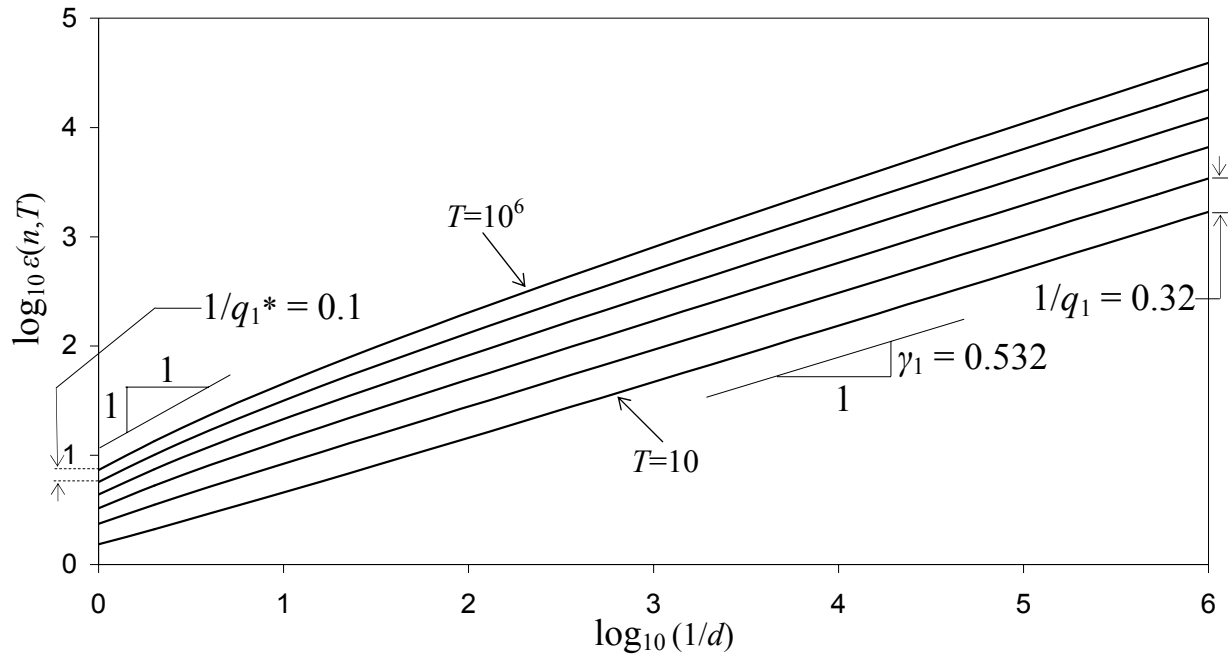


Figure 4: Return-period values $\varepsilon_{n,T}$ for a multifractal cascade with moment scaling function $K(q) = 0.1(q^2 - q)$. The plots show $\varepsilon_{n,T}$ against the averaging duration $d = m^{-n}$ for $T = 10, 10^2, 10^3, 10^4, 10^5$ and 10^6 cascade realizations (T increases from bottom to top).

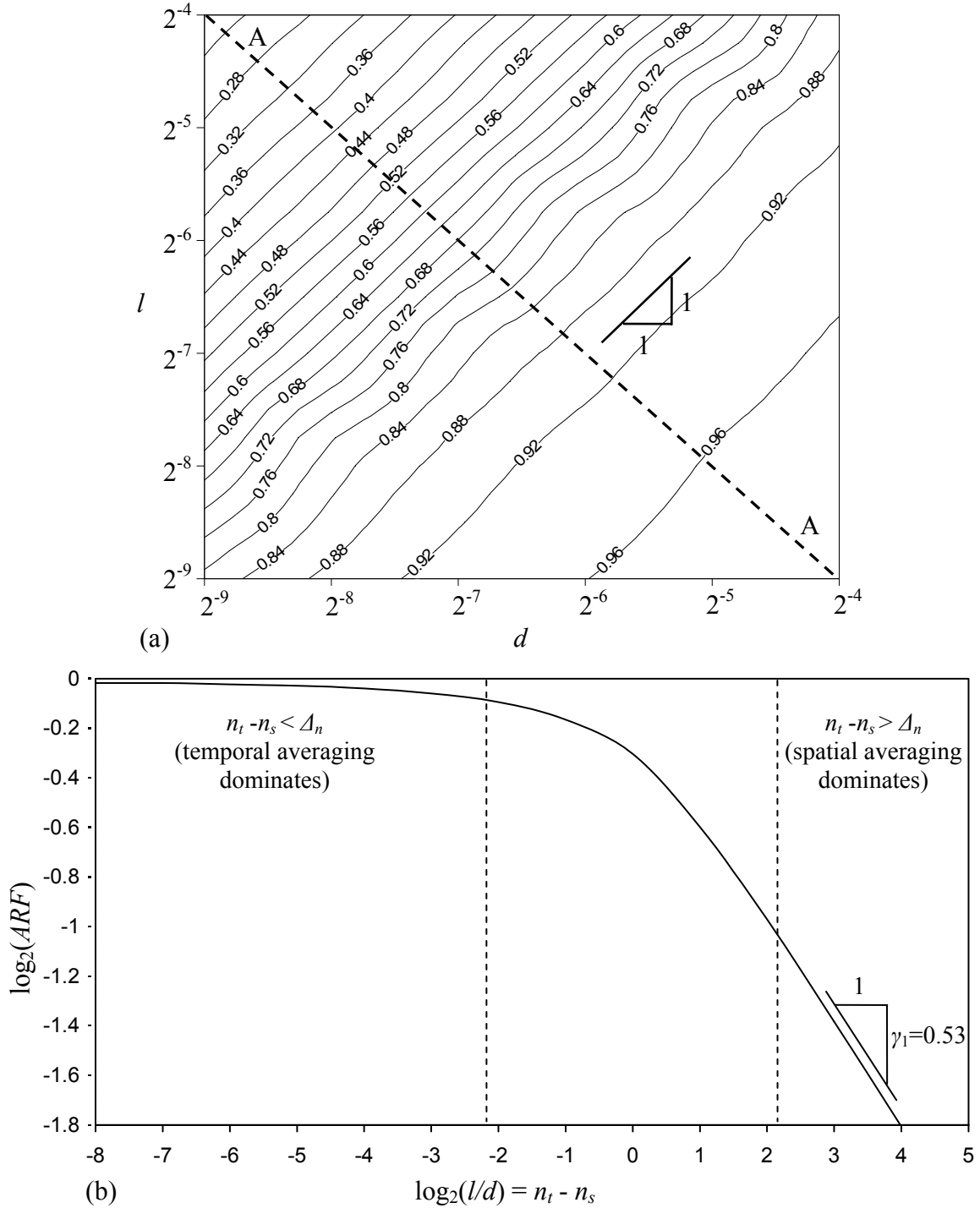


Figure 5: Idealization of rainfall as a discrete cascade inside the unit cube in (x, y, t) -space, with moment scaling function $K(q) = 0.1(q^2 - q)$. (a) Dependence of the areal reduction factor ARF on the side length l of the square averaging region and the duration d of temporal averaging. (b) Scaling of the ARF factor with the ratio l/d . For large l/d ratios, the ARF behaves like a power function of l/d , with exponent $-\gamma_1 = -0.532$.

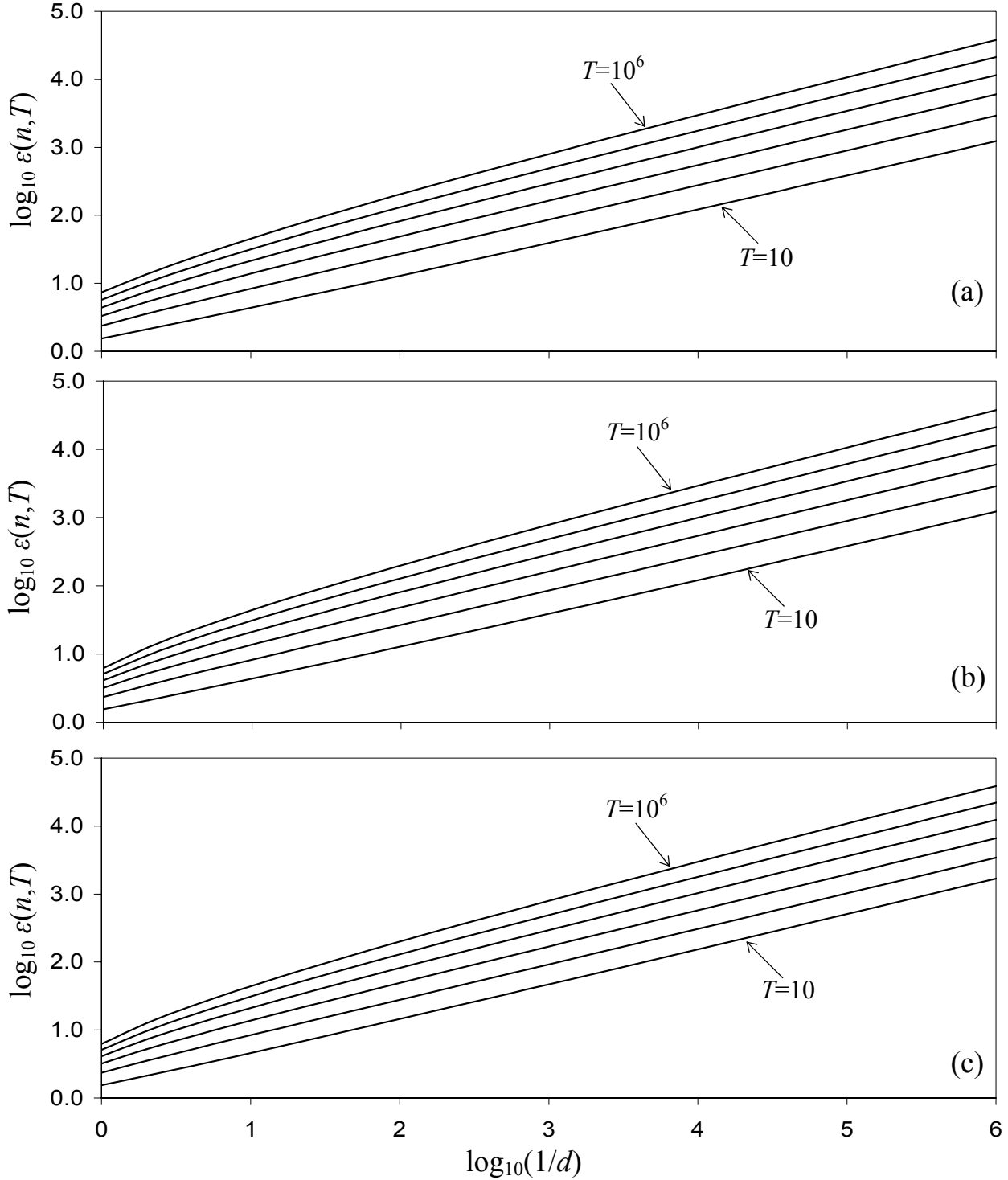


Figure 6: Return-period values $\varepsilon_{n,T}$ for the multifractal cascade used in Figure 4: (a) exact values using the distribution of $\varepsilon_{n,\max}$, (b) approximation when Z is replaced with A_{r_Z} using a second-moment matching criterion ($r_Z = 2.237$), and (c) approximation when, in addition, one neglects dependence among the cascade tiles. Return periods are $T = 10, 10^2, 10^3, 10^4, 10^5$ and 10^6 cascade realizations, increasing from bottom to top.

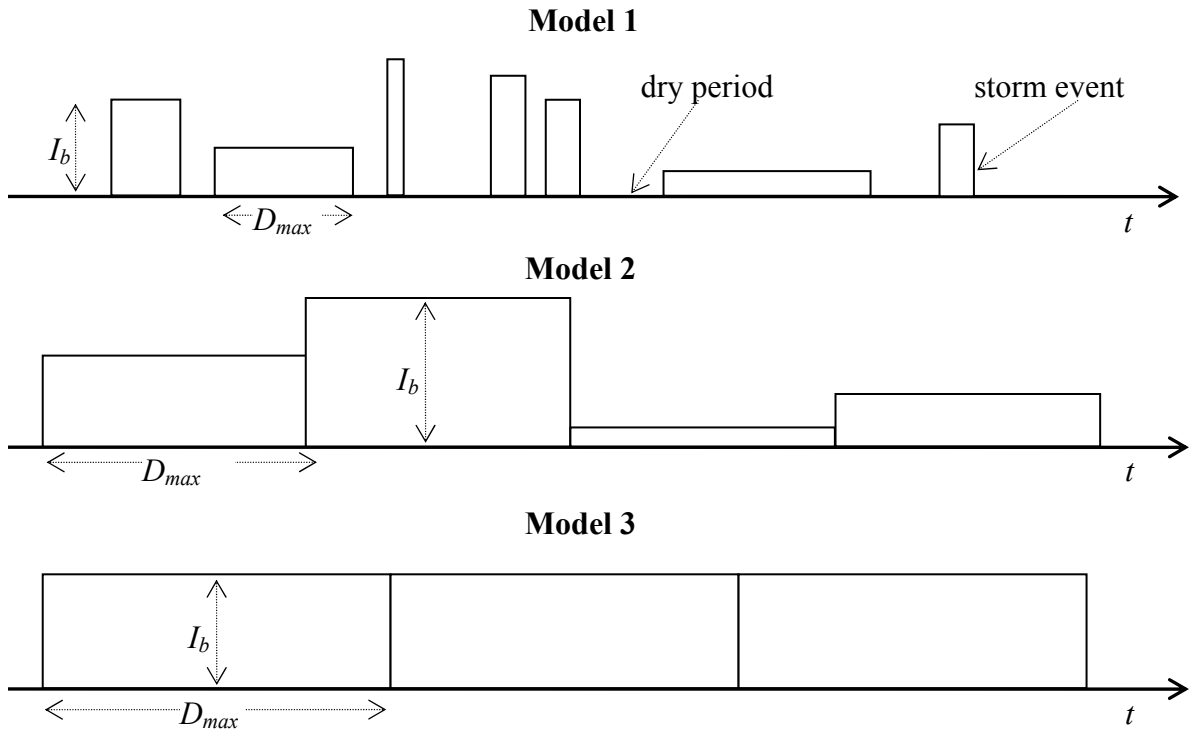


Figure 7: Schematic representation of the “exterior process” for rainfall models 1, 2, and 3. In all cases, the interior process is stationary multifractal with independent realizations inside different D_{max} intervals.

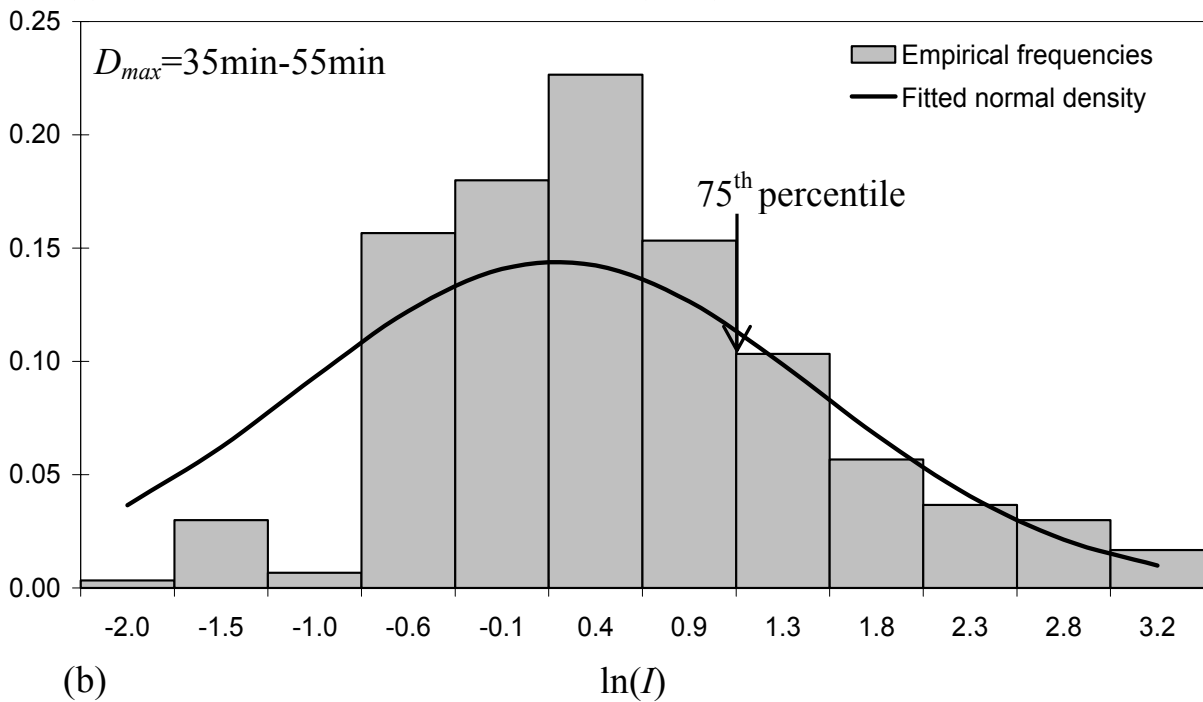
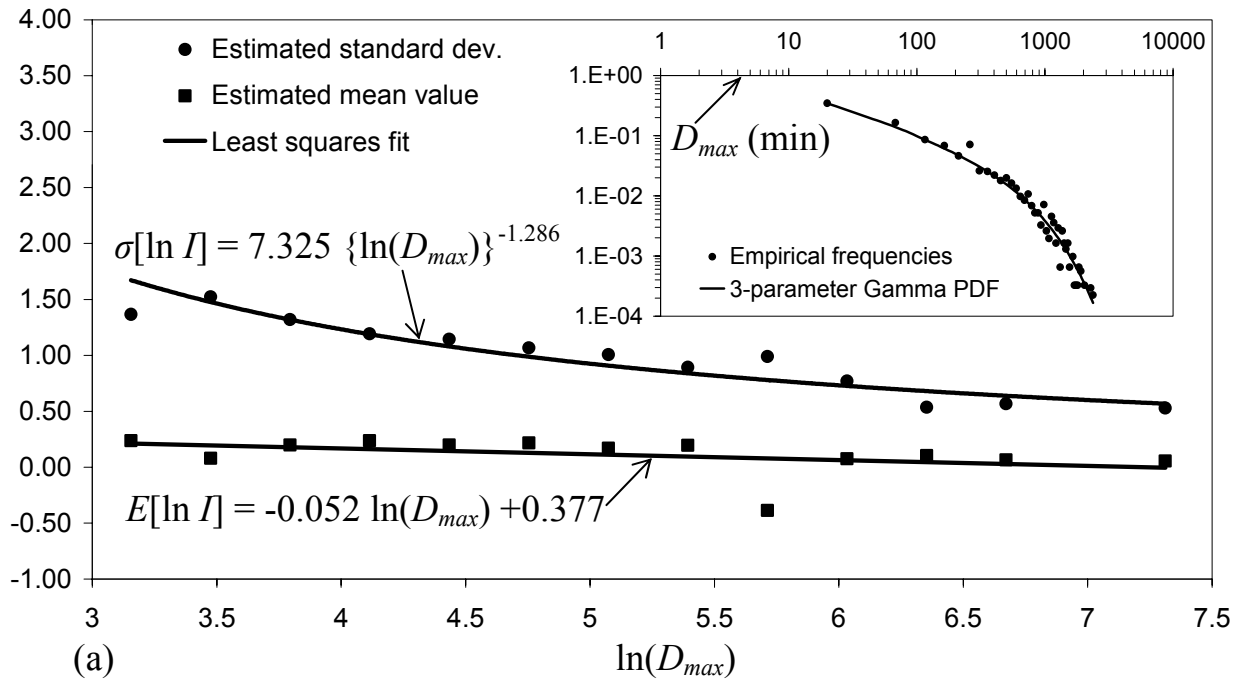


Figure 8: Use of Model 1 to evaluate the IDF curves for Florence, Italy, based on a 23-year record: (a) Fitted gamma distribution of storm duration D_{max} (inset) and mean and variance of the conditional log storm intensity ($\ln I | D_{max}$). (b) Example tail fit by maximum-likelihood of a normal distribution to $\ln(I)$ for D_{max} between 35 and 55 minutes.

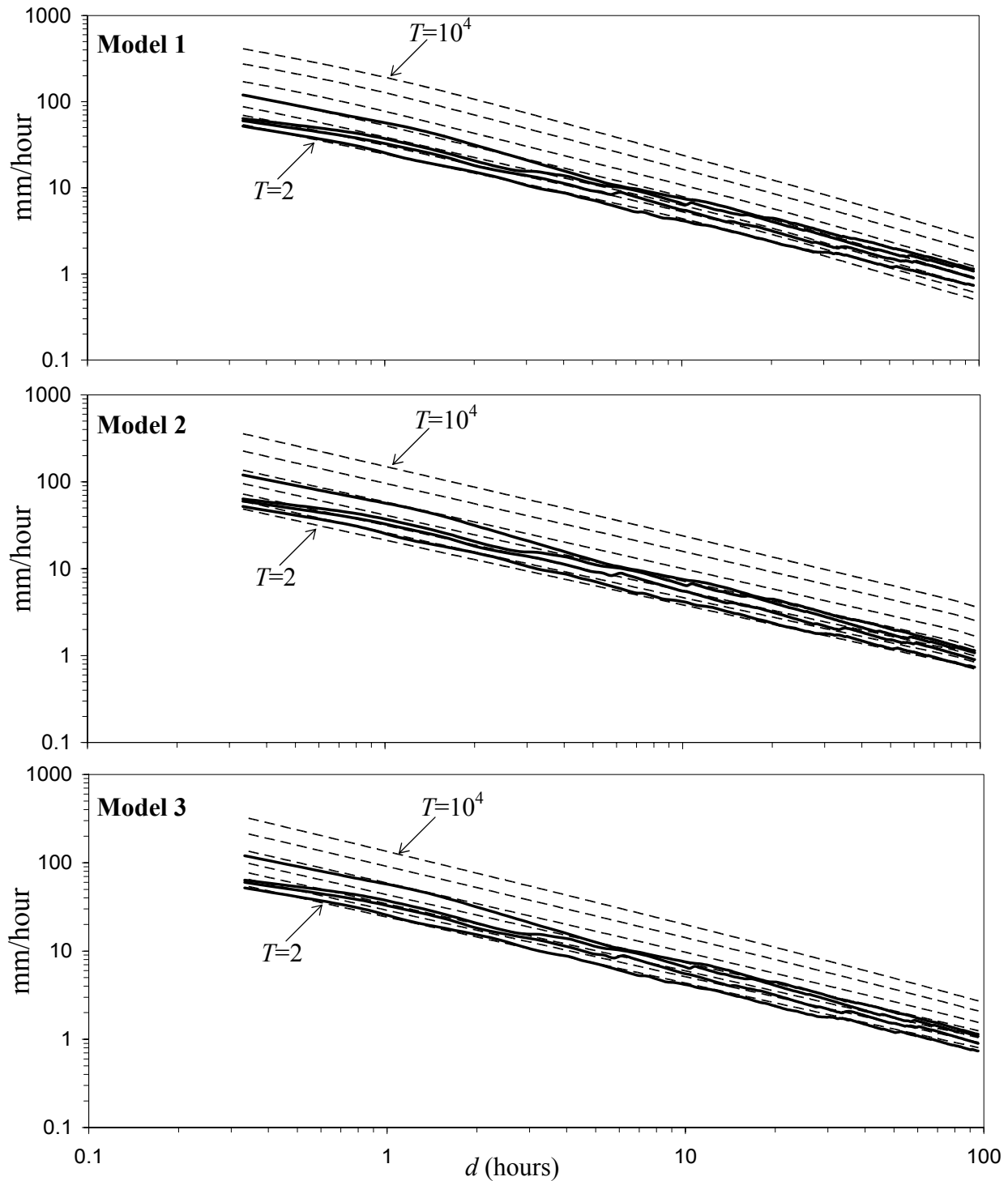


Figure 9: Comparison of model-generated IDF curves (dashed lines) and empirical IDF curves (solid lines) for Florence, Italy, using rainfall models 1, 2 and 3. The model-generated curves are for return periods $T = 2, 4, 8, 23, 10^2, 10^3$ and 10^4 years and the empirical curves are for $T = 2, 4, 8$ and 23 years, both increasing from below.